Università degli Studi di Cagliari

DOTTORATO DI RICERCA

Progettazione Meccanica

Ciclo XXVII

Analytical solutions of the steady or unsteady heat conduction equation in industrial devices: A comparison with FEM results.

ING-IND/09

Author dott. Ing. Bulut Ilemin

PhD coordinator Prof. Ing. Natalino Mandas

Supervisor Prof. Ing. Francesco Floris

Esame finale anno accademico 2014 – 2015

Acknowledgements

I would like to acknowledge everyone who has assisted me throughout my doctoral studies over the years. It would not have been possible to do without the support and guidance that I received from many people.

I am deeply indebted to my supervisor prof. Francesco Floris for his fundamental role in my doctoral work and who, as well, encouraged me to pursue my doctoral degree. I am very grateful for his patience, continuous support, valuable advices, enthusiasm, and immense knowledge.

I would like to express my gratitude to my colleagues Simone La Croce e Omar Caboni and all the Mechanical Engineering Faculty members from the University of Cagliari for their valuable contribution.

I am also very thankful to prof. Aleksandar G. Ostrogorsky for his welcoming support and valuable input during the time I spent in Illinois Institute of Technology.

I would like to take this public opportunity to specially thank to Egle for the love, encouragement and moral support throughout my research.

Finally, my deepest gratitude goes to my mother, my father and my sister, whose endless love and guidance are with me whatever I pursue.

Abstract

Heat transfer is one of the most salient and fundamental research areas for any engineer, due to its ubiquity. Today the energy efficiency requirements are becoming more and more demanding. This motivates engineers to continuously improve the efficiency of heat transfer processes.

For such analysis nowadays, the common and the popular practice to infer the temperature field is now commercially available in computer codes. Analytical solutions for the temperature field are also available under the assigned conditions such as Dirichlet, Neumann or Robin, if the thermal conductivity is constant and isotropic. In the cases where conductivity is anisotropic and strongly dependent by temperature or the material is not homogenous, the exact solution of the energy conservation in the body is not possible due to high non linearity in the equations.

Despite the complexity of many engineering structures, the present work is undertaken to demonstrate that the reduction to a simpler version of more complex heat conduction equations is possible and the exact analytical solution is comparable with the approximate finite element solution.

The topic of the present research study is the resolution of the problems in various engineering fields through the analysis of conduction heat transfer in rigid bodies, transition bodies, steady and transient bodies and the provision of analytical solutions with graphical representation of the results. Namely; in an electrolytic capacitor, a food container and a gas turbine blade. The modelling of them plays an important role because excessive temperatures drastically reduce the lifetime of capacitors, turbine vanes and blades. In the food sterilization it is necessary to know the thermal wave behaviour in order to reduce its associated costs or to guarantee the sterilization time.

The last part of this study is the evaluation of the numerical simulation results in order to make a comparison with the analytical results and, when possible, with experimental data. For such analysis a finite element method has been utilized by both commercial and free software; namely, ANSYS™ and FreeFem++. Very good agreements are obtained between both of them.

Contents

List of figures

Chapter 1

General Introduction

1.1 General motivation and objective

For all engineers heat transfer is a fundamental research area, since it is ubiquitous. The increase in demand for implementation of new and efficient energy techniques motivates engineers to propose ideas to improve the efficiency of heat transfer processes. Over the past years a large quantity of equipment that relies on heat transfer phenomena has been developed and improved significantly.

In complex geometries where the conduction is stationary or transient, with or without production of internal heat in objects subjected to the various boundary conditions, heat flow assigned or Robin or in combination between them, or the Neumann or Dirichlet, is established practice to calculate the temperatures of finite element (FE) now commercially available and widely applicable.

Analytical solutions are also available for stationary and transient cases cylinders and collars (extended surfaces) under the conditions of radiation and convection board (Robin), if the thermal conductivity is constant and isotropic [1], [2], [3], [4], [5].

In cases where the conductivity is anisotropic and a strong function of temperature, or the material is not homogeneous, an exact solution does not exist. Despite many structures of interest, the mechanics are of complex geometry, or the material is of a very viscous consistency, such as in foods to be sterilized, it has been shown that the reduction of the heat transport equations to simpler shapes is possible, in which is located an explicit solution with the solutions that are comparable to those of the finite element modeling. Which allows a greater adherence to both the geometry and the real properties of the material.

This work is based on two parts: the first main part is the study and the analysis of analytical conduction heat transfer models in order to simulate the temperature

distribution based on energy balance. Second part is the numerical modelling which are implemented in ANSYS Multiphysics and FreeFem++ packages in order to validate those obtained results from the analytical solutions.

1.2 Thesis outline

This Thesis is structured in four chapters subdivided in paragraphs for each topic. The following chapter is aimed to give a background to the heat conduction equation analysis. Chapters 3, 4 and 5 are the main parts of this present work, being each free standing. The contents of the Thesis and chapters progress in stages from an introduction to an advanced level.

In addition, Chapters 3, 4 and 5 have their own introduction, body and conclusion parts. The structure for all of them is organized as;

- First is to give a brief introduction to the related engineering areas.
- Subsequently, next is to describe physically and mathematically the interested model and developing the analytical models to obtain an exact solution.
- Third is providing numerical solutions by utilizing finite element method, where the space continuum is partitioned into finite number of elements, in order to compare to the analytical results.
- The part of final is to discuss the results and to make a comparison between analytical and numerical results, and, when possible, with experimental data.

A brief description of each chapter is given as follows:

Chapter 2 gives a quick introduction on the basis of heat conduction equation.

Chapter 3 thinks about the electronic industry devices. More specifically it deals with analysis of conduction of heat transfer within capacitor by considering heat generation due to joule effect. The case is considered to be independent by time. An electric circuit was set up in order to check the superficial temperature of the capacitor under assigned convection heat transfer through ventilation. Subsequently, a full 3D finite element method through ANSYS™ is performed in order to make a comparison between the results of the analytical and numerical solutions.

Chapter 4 considers the food processing industry. It addresses the presentation of an exact solution of temperature field in the sterilization of a tinplate can under transient heating stage. The analytical solution is obtained based on the separation of variables in space and time. A finite element analysis is made through the software; namely, ANSYS™. Lastly, the results of analytical and numerical solutions is compared with the experimental data.

Finally, **Chapter 5** is oriented to the thermal analysis of gas turbine blades. It introduces how to model a gas turbine blade being cooled from its base while receiving convection and radiation heat from combustion products. The difficulty of analytical solution arises from the modelling of its form, which causes to it to reduce its thickness between the leading edge and the trailing edge, furthermore from the necessity of bringing the thickness of the blade at the end to zero. The energy balance is modeled in the form of 2D elliptical however, in a type of degenerative elliptical since there is a missing boundary condition. As a first approach, an exact solution is found through the sum of the functions by considering that there is no internal cooling. This case is also studied as a full 3D model with a commercial finite element code ANSYS™ in order to make a comparison with the analytical results. As a next step, the turbine alloy is considered to be internally cooled due to the use of compressor air bled from the intermediate stages of the compressor. With the hypothesis of heat sink or “law of cooling, a solution method of energy balance in the alloy is obtained through the finite element method by FreeFem++ software.

1.3 **Publications**

Some of the topics discussed in this thesis have been already published in international journal, and presented at national and international conferences. This thesis is based on the following published articles.

International Journal Papers:

1. Floris F, Orru P, Ilemin B., *Quasi 1-D analysis of Heat Equation with exact solutions and comparison with numerical simulation in liquid/vapour pressure tanks, waterwalls and hot-drawing machines.* 31st UIT Heat Transfer Conference. 2013. p. 87-97.
2. Floris F, Ilemin B, Orrù P., *A Multi-dimensional Heat Conduction Analysis: Analytical Solutions versus F.E. Methods in Simple and Complex Geometries with Experimental Results Comparison.* Energy Procedia. 2015;81:1055-1068.
3. Floris F. and Ilemin B., *Analytical Solution on cooled turbine blade under parallel convective and radiation heat flux at leading edge and suction/pressure side*, Atti del 33rd UIT National Heat Transfer Conference, 22-24 Giugno 2015, L'Aquila, Italia.
4. Floris F. and Ilemin B., "*Soluzioni esatte e soluzioni numeriche della conduzione termica nell'industria alimentare, in condensatori commerciali e nelle pale di turbina"*, La Termotecnica ricerche tecnologie impianti, Dicembre 2015 N° 10, pp.45-50.

Chapter 2

Preliminaries

2.1 Introduction

PRIMARY causes are unknown to us; but are subject to simple and constant laws, which may be discovered by observation, the study of them being the object of natural philosophy.

Heat, like gravity, penetrates every substance of the universe, its rays occupy all parts of space. The object of our work is to set forth the mathematical laws which this element obeys. The theory of heat will hereafter form one of the most important branches of general physics.

— Joseph Fourier, The Analytical Theory of Heat

Energy exists everywhere within the universe and there is no doubt about its importance. It can be shortly defined as the ability for doing work or making a change, whereas work can be defined as the transfer of energy. The presence of energy can be in a variety of forms, such as nuclear, mechanical, electrical, chemical, gravitational and thermal.

As the first law of thermodynamics describe how energy cannot be created or destroyed; the total amount of energy is fixed within the universe and it can be merely transferred or transformed from one form to another form using fundamental interactions.

Heat is a salient form of energy and simply defined as the transfer of energy as a result of temperature difference. The second law of thermodynamics implies that the movement of heat is from the hotter body to the colder body in the existence of a temperature difference within a thermally insulated system from its surroundings.

There are three primary mechanisms of heat transfer; namely conduction, convection and radiation.

Conduction heat transfer is perhaps the most frequently encountered type, and occurs regularly in nature. In short, it is the transfer of heat by the energy of motion between adjacent atoms or molecules, the temperatures tend to equalize between molecules.

Convection involves the transfer of heat by bulk transport and the mixing of macroscopic particles of hot and cold elements of a liquid or gas.

Radiation heat transfer differs from conduction and convection heat transfer since it does not rely upon any contact between the heat source and the heated object. Hence no physical medium is required in the process of radiation. The heat is transferred by electromagnetic radiation that involves waves (or quanta).

2.2 **Differential formulation of energy conservation law**

The differential form of the energy conservation equation may be obtained using two different methods. One of these methods is directly applying the first law to an appropriately chosen differential control volume, while the second method starts with the integral form of the first law for an arbitrary system. [2] The latter method, being more general and more mathematically elegant, is preferred to present here.

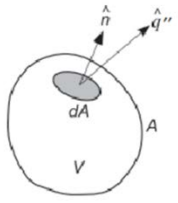

Fig. 1- An arbitrary control volume.

For an arbitrary small control volume, as shown in figure (1), a statement of law of conservation energy may be expressed as [5]

$$\begin{bmatrix}\text{Rate of energy}\\ \text{storage in V}\end{bmatrix} = \begin{bmatrix}\text{Rate of heat entering}\\ \text{through the boundaries of V}\end{bmatrix} + \begin{bmatrix}\text{Rate of energy}\\ \text{generation per unit time}\end{bmatrix}$$

The first term on the right side that is the rate of heat entering into the volume element may be conveniently written in integral form as

$$-\int_A \mathbf{q}\cdot\mathbf{n}dA = -\int_V \nabla\cdot\mathbf{q}dV \qquad [1.1]$$

where;

- q″ = the heat flux vector at *dA*.
- n = the outward-drawn normal vector to the surface element *dA*.
- V = small volume element of the system,

and the area integral is converted into a volume integral by using the divergence theorem of vector calculus. Similarly, the rate of heat generation can also be written in integral form

$$\int_V Q_{gen}dV \qquad [1.2]$$

where;

- Q_{gen} = the heat generation within the system.

Before evaluating the rate of heat energy storage, it is convenient to define the material derivative term [5]. This can be written for a general property A as

$$\frac{DA}{Dt} = \frac{\partial A}{\partial t} + \mathbf{V}\cdot\nabla A \qquad [1.3]$$

where the term on the left side is called the material derivative of property A, and the terms on the right hand sides are called the partial time derivative and the convective derivative of property A, respectively. And V is the velocity vector which has components of v_x, v_y, v_z.

By introducing the Reynolds transport theorem it is possible to calculate the material derivative of a volume integral. Thus, for a general property A, the rate of heat energy storage within the volume can be expressed. First, letting $A(r,t) = \rho cT(r,t)$ and also considering the definition of the specific heat at constant volume [2], the heat storage term can be expressed as an integral, which is

$$\int_V \rho c\left[\frac{\partial T}{\partial t} + \nabla\cdot\left(T\ \mathbf{V}\right)\right]dV \qquad [1.4]$$

Thus, substituting equations (1.1), (1.2), (1.4) into the statement equation and rearranging all these equations into one common integral, energy conservation equation appears as

$$\int_V \left(\rho c \left[\frac{\partial T}{\partial t} + \nabla \cdot \left(T \ \mathbf{V} \right) \right] + \nabla \cdot \mathbf{q} - Q_{gen} \right) dV = 0 \qquad [1.5]$$

Since equation (1.5) is derived for an arbitrary small volume element, so that the only way it is satisfied for all choices of volume is if the integrand itself is zero. Thus eliminating the volume integral operation yields

$$\rho c \left[\frac{\partial T}{\partial t} + \nabla \cdot \left(T \ \mathbf{V} \right) \right] = -\nabla \cdot \mathbf{q} + Q_{gen} \qquad [1.6]$$

That is the differential equation for energy conservation within the system. It is not of much use in the present form since it involves variables, however, it is the starting point to derive the differential form of the equation of conduction.

Fourier's Law of Conduction

Microscopic theories such as the kinetic theory of gases and the free-electron theory of metals can be used to predict the conduction through media. However, the macroscopic or continuum theory of conduction disregards the molecular structure of continua. Thus conduction is taken to be phenomenological and its effects are determined by experiments [1], [2].

Fourier's law of conduction, which is an empirical law based on observation, describes the relationship between the heat flow and the temperature field. This particular law is named after French mathematician and physicist Joseph Fourier in 1822 [1], [2] and may be given in the following vectorial form

$$\mathbf{q}'' = -k \ \nabla T \qquad [1.7]$$

Where the temperature gradient is a vector normal to the isothermal surface and the heat flux vector q'' represents the heat flow per unit time, per unit area of the isothermal surface in the direction of the decreasing temperature. The quantity k is called the thermal conductivity of the medium, and has units of $Wm^{-1}K^{-1}$.

Unlike the first law of thermodynamics, Fourier's law does not have the same 'legal' standing. Equation (1.7) presents a phenomenological linear relationship between q''

and ∇T, which will be highly accurate providing that the characteristic length scale of the temperature gradient is significantly larger than the microscopic length scale of the medium. Practically, all engineering applications fall into this category except the cases such as boundary layer in a space vehicle.

2.3 **Equation of conduction**

Introducing Fourier's law of conduction into the law of conservation of thermal energy eliminates the heat flux term simultaneously provides the differential form of the heat conduction equation. Since our interest lies in solids or an incompressible medium whose continuity is 0, therefore, by the means of the well-known vectorial identity above expression can be introduced into equation (1.6) and the desired heat conduction equation in cartesian coordinates can be expressed as

$$\rho c\left[\frac{\partial T}{\partial t}+v_x\frac{\partial T}{\partial x}+v_y\frac{\partial T}{\partial y}+v_z\frac{\partial T}{\partial z}\right]=\nabla\cdot\left(k\nabla T\right)+Q_{gen} \qquad [1.8]$$

This equation is valid in the case of constant (ϱc) for an incompressible, moving solid with velocity *V*. The heat conduction equation can be expressed in several different forms. For stationary solids when the thermal conductivity is constant, above expression simplifies to

$$\frac{1}{\alpha}\frac{\partial T}{\partial t}=\nabla^2 T+\frac{Q_{gen}}{k} \qquad [1.9]$$

where α is the thermal diffusivity of the material which has units of (m^2/s) and defined as

$$\alpha = k/\rho c \qquad [1.10]$$

On the other hand, the particular form of the Laplacian operator depends on the coordinate system. There are 11 orthogonal coordinate systems in the Laplacian can be cast as a differential operator. For the most common geometries of cartesian, cylindrical and spherical, the Laplacian is

$$\begin{aligned}
\nabla^2 T &= \frac{\partial^2 T}{\partial x^2}+\frac{\partial^2 T}{\partial y^2}+\frac{\partial^2 T}{\partial z^2}\\
\nabla^2 T &= \frac{1}{r}\frac{\partial}{\partial r}r\frac{\partial T}{\partial r}+\frac{1}{r^2}\frac{\partial^2 T}{\partial \phi^2}+\frac{\partial^2 T}{\partial z^2}\\
\nabla^2 T &= \frac{1}{r^2}\frac{\partial}{\partial r}r^2\frac{\partial T}{\partial r}+\frac{1}{r^2\sin\theta}\frac{\partial}{\partial \theta}\sin\theta\frac{\partial T}{\partial \theta}+\frac{1}{r^2\sin\theta}\frac{\partial^2 T}{\partial \phi^2}
\end{aligned} \qquad [1.11]$$

General Initial and Boundary Conditions

- **Initial (volume) condition**

For transient problem the temperature of a continuum under consideration must be known at some instant of time. In many cases this instant is most conveniently taken to be the beginning of the problem. Mathematically speaking, if the initial condition is given by $T_0(r)$, the solution of this problem, T(r, t), must be such that at all points of the continuum

There are several boundary conditions encountered in conduction heat transfer, some of the formal ones are as follows.

- **(1) 1st type of boundary condition (Prescribed Temperature).**

This is the first and most basic type of boundary condition where the temperature is prescribed to be a constant or a function of space and/or time at the surface of the system. Mathematically these can be shown as respectively

$$T\big|_{surface} = T_0 \quad \text{or} \quad T\big|_{surface} = f\left(\hat{r}, t\right)$$

where T_0 is the known boundary temperature as a constant, while *f(r, t)* is the prescribed surface temperature distribution as a function of both space and time. Mathematically speaking, boundary conditions of the first type are called Dirichlet boundary conditions.

- **(2) 2nd type of boundary condition (Prescribed Heat Flux).**

The second type of boundary condition is specified heat flux at the surface that is to be a constant or a function of space and/or time. These can be shown as follows

$$-k\frac{\partial T}{\partial n}\bigg|_{surface} = q_0'' \quad \text{or} \quad -k\frac{\partial T}{\partial n}\bigg|_{surface} = f\left(\hat{r}, t\right)$$

where q_0'' is the applied constant heat flux, *f(r, t)* is the prescribed surface heat flux as a function of both space and time and ∂T /∂n is the derivative along the outward-drawn normal to the surface as shown in fig (a). If the derivative is along the inward-drawn normal to the surface, the sign of the derivative would be minus. Thus, it is important to write a more general form

$$\pm k \left.\frac{\partial T}{\partial n}\right|_{surface} = \pm q''$$

The plus and the minus signs of the left hand side of this equation correspond to the differentiations along inward and outward normal respectively, and the plus and minus signs of the right hand side correspond to the heat flux from and to the boundary, respectively. These are shown in the figure (2).

Mathematically speaking, boundary conditions of the second type are called Neumann boundary conditions. A special and common form of this boundary condition appears when the heat flux is equal to zero.

$$\left.\frac{\partial T}{\partial n}\right|_{surface} = 0$$

which is called either adiabatic or perfectly insulated surface.

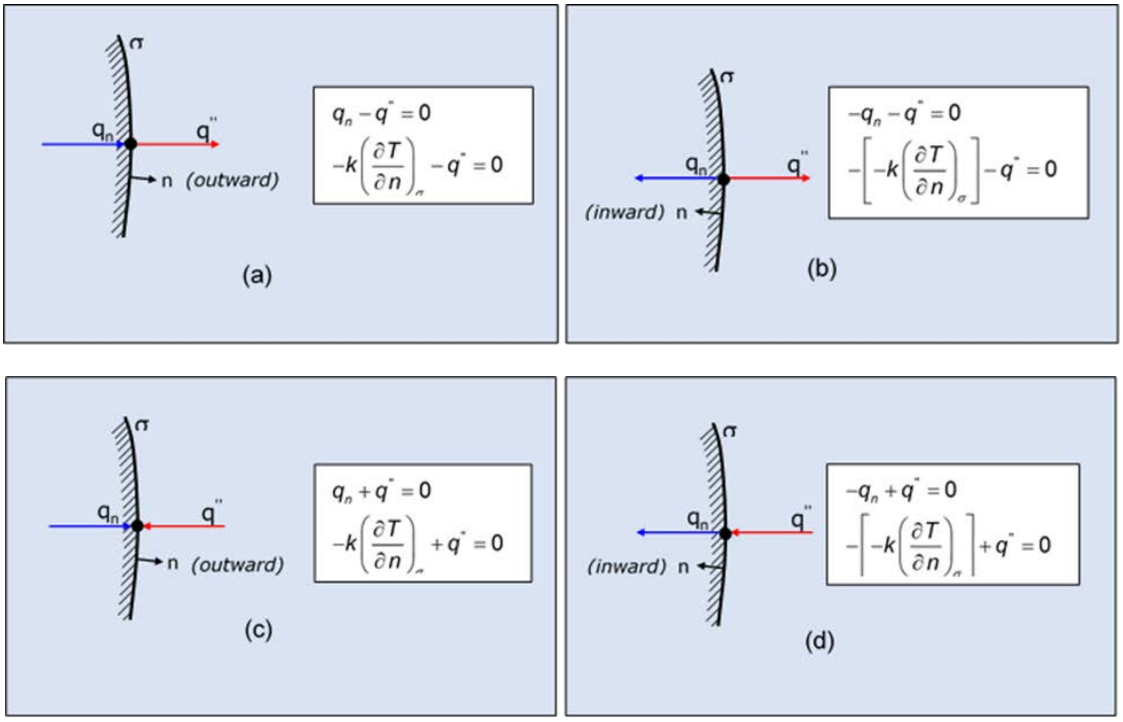

Fig. 2- Directions of second kind of boundary conditions.

- **(3) 3rd type of boundary condition (Convection condition).**

The third type of boundary condition also referred to as the convection condition is obtained from the Newton's law of cooling, that is, the heat flux to or from the

surface of a boundary is proportional to the difference between the boundary temperature and the ambient temperature as follows

$$\pm k \left.\frac{\partial T}{\partial n}\right|_{surface} = h\left(T_\sigma - T_\infty\right)$$

where T_σ is the boundary temperature, T_∞ is the ambient temperature and the quantity h is the convection heat transfer coefficient. Again in this equation the minus and positive signs play critical role, as shown in the figure (3).

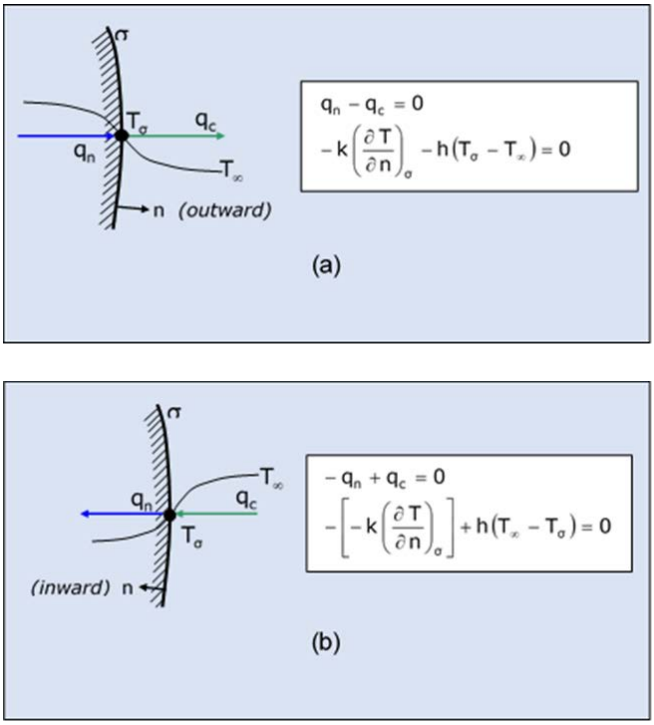

Fig. 3- Third kind of boundary conditions.

- **(4) Radiation condition.**

When the surface temperature are relatively high, heat transfer by radiation rapidly increases thus, it becomes significant. It may contribute up to fifty percent of the total heat transfer. The net radiation heat flux between a surface and its surrounded environment may be typically expressed as

$$q''_{rad} = \varepsilon\sigma\left(T_{\sigma}^{4} - T_{\infty}^{4}\right)$$

where ε is the emissivity of surface, σ is the Stefan-Boltzmann constant that is equal to 5.67 10^{-8} ($Wm^{-2}K^{-4}$) and T_{∞} is the ambient radiation temperature. This boundary condition is a bit complex due to the non-linearity, because the dependent variable temperature appears in the fourth power.

- **(5) Other Boundary Conditions.**

Except above boundary conditions, the most frequently used ones during the solution of the heat conduction equation are symmetry condition which acts like an adiabatic, interface boundary conditions when the two materials are having different conductivities. Another one to consider here may be the necessity for finite temperature throughout the domain of a problem. For instance, with curvilinear coordinate systems, the solution of the heat equation often contains functions that tend to infinity as their argument approaches to zero.

2.4 Quasi 1D-analysis of heat conduction equation

There are many engineering thin devices subjected to heat transfer from both sides whose solid temperature distribution may be inferred by the extended surface (fin) analysis through the solution of the energy equation in quasi 1-dimension, steady or transient state.

In a few cases it is possible to use a simple analytical solution of the energy equation if the numerical analysis of the complex 2-D or 3-D modelling -that takes into account more spatial parameters and dependence from temperature of major physical parameters- gives minor differences in the field temperatures. For instance;

- *Pressure tanks :* An uneven distribution of temperature in pressure tanks (pressured liquid gas, natural gas for automotives), boiler drums and slag tap cyclones (both in steam generating units), as show in figure (4), is possible when the vapour and liquid volumes have a defined separation surface between the phases. The values of vapour - side and liquid-side heat transfer coefficients may vary of two orders of magnitude. The determination of temperature field in the metal body can be obtained via a quasi 1-D treatment of the heat equation, assuming that the thermal conductivity is independent of temperature.

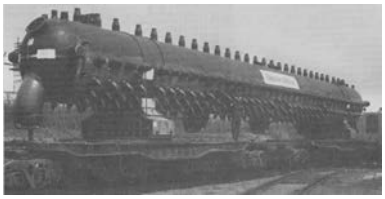

a) Steam drum of a flat car en route to a power plant construction site. Courtesy of Babcock&Wilcox.

b) Liquified petroleum gas tanks.

c) In automotive industry.

Fig. 4- Examples of pressure tanks and steam drums.

- *Waterwalls*: They are exposed to quite different heat fluxes on a side due to heat release zone position and convective heat transfer on the other side due to nucleate boiling. On a vertical elevation of more than 30 meters, conduction through the metal is possible due to changes in metal temperature. Due to low thickness (a few mm) of tubes compared to the highness of waterwall (longer than 30000 mm), a quasi 1-D of an infinite plate is feasible. An illustration is shown in figure 2.

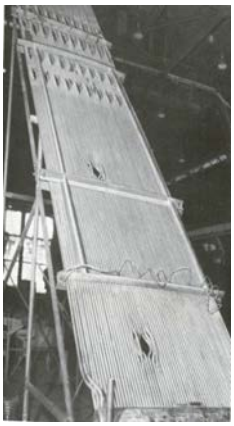

Fig. 5. Example of waterwalls. (Photo courtesy of Babcock&Wilcox).

- *Extrusion:* In the extrusion of thin hot plates through rotating dies, as shown in figure (6), the heat transfer from metal (or plastic sheet) to a cooler fluid at known convective heat transfer coefficient vented across the slab may be treated as an extended surface quasi 1-D. In order to calculate the angular velocity of dies the temperature field has to be established with solution of heat equation integrated with entalphy flux. Péclèt number is the key parameter in the exact solution.

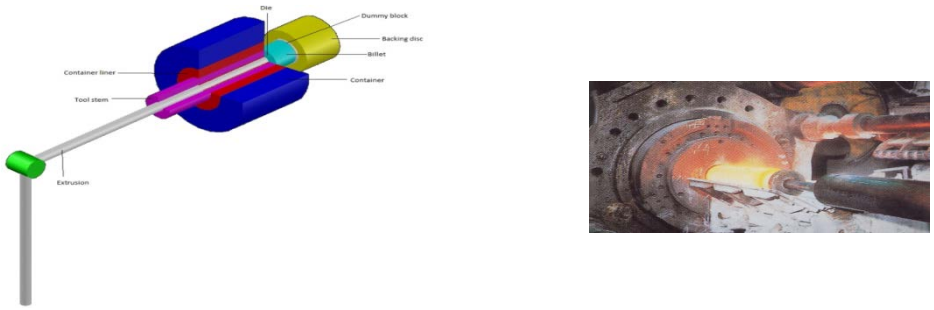

Fig. 6 - Examples of extrusion processes.

Above examples are just some of the cases that the temperature distribution may be easily inferred by the extended surface (fin) analysis through the solution of the energy equation in quasi 1-dimension for either steady or transient state.

In the first published paper, various comparative examples involving rectangular and cylindrical coordinates of water walls, tanks and extrusion sheets with incompressible fluid flow at high Péclet number are analyzed. Then, the results of these exact solutions are compared to the finite element analysis, which take account of the variability of thermo-physical properties with temperature and dimensionality whose analytically complex differential equations with temperature built-in functions cannot be solved with explicit solutions. Their results were in a very good agreement in each case.

The modeling studies were then focused on the solution of more complex conduction cases, with / without internal heat production, and in steady and transient conditions as in electrical capacitors and commercial foods compressed into cakes under sterilization with wet steam in an autoclave. These are presented in the following chapters 3 and 4, respectively.

Chapter 3

Thermal modelling of a capacitor

3.1 Introduction

Capacitor, formerly referred to as a condenser, is a widely-used and passive electronic component or device that is capable of storing energy in the form of an electrostatic field.

The history of the theory of capacitors technology is quite old and dates back to the invention of the Leyden jar. According to the literature, the Leyden jar was discovered almost simultaneously by German cleric Georg von Kleist in 1745 and Dutch physicist Pieter van Musschenbroek, in the University of Leyden, in 1746 [6]. As originally constructed, it consisted of a glass jar partially filled with water with an electrical lead passing through a cork in the top of the jar to the water [7]. The wire lead was then hooked up to an electrostatic generator, which served as a source of electricity. At first, experimenters thought that the charge was held in the water, but through experimentation Benjamin Franklin figured out that the water in the jar was not essential and could be replaced by attaching an electrode to the inside of the jar since the basic requirement for a functioning Leyden jar is the presence of two conductors separated by an insulator. And then, Leyden jars evolved over time into more efficient devices. Some demonstrations of Leyden Jars are given in figure (7).

Fig. 7- Some Leyden jars. (Courtesy of John Jenkins, www.sparkmuseum.com.)

As the precursor to the modern capacitors, knowledge of the Leyden jars quickly spread to the laboratories; since then, there has been stupendous progress in the technology of capacitors. In the early times, these devices were mainly used in electrical and electronic products, however, nowadays they are used almost everywhere, in the fields ranging from industrial application to automobiles, aircraft and space, medicine, computers, games and power supply circuits [8].

Thus, there are a great variety of different kinds of capacitors available used in the market depending on their ancestry and applications. However, all of their essence is the same thing; namely, stores the charge.

3.2 **Fundamentals of Capacitor**

Fundamentally, they are composed of two or more parallel conducting plates separated either by air or by an insulated material for accumulating electrical charge. The insulator is properly called dielectric. While the dielectric material can theoretically be any non-conductive substance, in practical applications, specific materials such as glass, vacuum, mica, ceramic, plastic, aluminum, and etc., are used depending on which best suit the capacitor's function. In this way each type has its own combination of features that makes it beneficial and important for some applications, while it can be inadequate for other applications.

The main purpose of capacitors is storing charge. However they can be used for various task in electrical circuits. These uses includes:

- Timing devices. This is due to the fact that the time needed to charge them is certain and can be predicted.
- Filters. They can be used as circuits that allow only certain signals to flow.
- Smoothing the voltage in circuits.
- Tuning. In radios and TVs.
- As batteries (large super-capacitors).
- Variety of other purposes.

As J.Ho et.al (2010) describes as that “Capacitors are a good example of the fact that even the simplest device can become complex given 250 years of technical evolution.”

On the other hand, the uses of small and large capacitors differ. Small capacitors can be used in electronic devices for various purposes such as coupling signals between

stages of amplifiers. Or they can be part of power supply system used to smooth rectified current. While large capacitors are mostly used for energy storage. They can be found in applications as strobe lights, as well as in some types of electric motors.

Capacitors can be standard (having a fixed value of capacitance) or adjustable. The latter capacitors are more frequently used in tuned circuits. The symbols for a fixed capacitor and an adjustable (variable) capacitor used in electrical circuit diagrams are shown in figure (8).

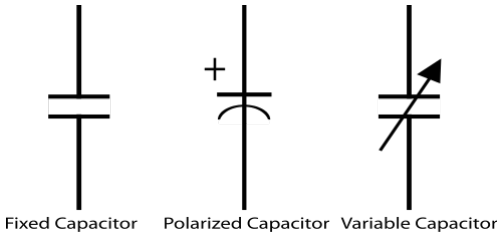

Fig. 8- Schematic symbols of capacitors.

Some of the most common capacitor types which find widespread application in electronics as well as electrical industries are Paper, Mica, Ceramic, Electrolytic, Tantalum, Power, Spherical, Super-capacitors, and others as shown in figure (9).

Fig. 9- Some different type of capacitors.

The Capacitance of a capacitor

Capacitance (*C*) is the measure of a capacitor's ability to collect and store energy in the form of electrical charge required for generating a unit potential difference between its plates [9]. In an ideal capacitor, the capacitance is defined as

$$C = \frac{Q}{V}$$

where Q is the electric charge stored in coulombs and V is the potential difference between the capacitor's plates in volts. The standard unit of capacitance is named Farad (F), which is really equivalent to coulomb/volt, in honor of British electrical pioneer Michael Faraday.

One farad is too great a unit of measurement to use in practical purposes, hence fractional values of Farad are almost always used such as micro-farads (μF), nano-farads (nF), pico-farads (pF) and so forth on. A large capacitance means that more charge can be stored. Super-capacitors, meanwhile, can store very large electrical charges of thousands of farads.

Parallel Plate Model

In a parallel-plate capacitor, as shown in figure (10), experiments demonstrate that capacitance C is proportional to the area A of a plate, inversely proportional to the plate spacing d (i.e. the dielectric thickness) and depends on the nature of the dielectric

$$C = \frac{\varepsilon_0 \varepsilon_r A}{d}$$

where;

- ε_0 is a constant value equal to 8.85 10^{-12} (F/m).
- ε_r is the relative permittivity.
- A is the area of the plates.
- d is the thickness of dielectric.

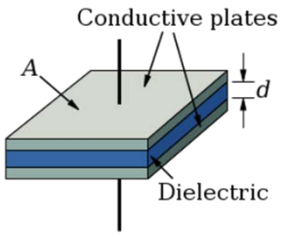

Fig. 10– Parallel plate (prototypical) model.

Aluminum Electrolytic Capacitors

Among other types of capacitors, aluminum electrolytic capacitors own a special position in numerous power applications and systems because they are very cost effective and able to provide a higher capacitance per volume (CV) compared to other types of capacitor. Therefore, these components are extensively preferred to use as power supplies wherein high volumetric efficiency is required such as aircrafts, space vehicles, automobiles, computers, mobile phones and many other electronics.

An aluminum electrolytic capacitor generally consists of a cylindrical wound capacitor element and impregnated with an electrolyte. The element is comprised of an anode foil, a cathode foil and paper separators which are saturated with a liquid or gel-like electrolyte [10]. The two foils are made of aluminum that gives rise to the fact that the capacitor is referred to as the aluminum electrolytic capacitor. The anode foil is usually highly etched to increase the plate's surface and there is a thin dielectric layer of aluminum oxide on the surface of the anode. The paper spacer is placed between them in order to prevent a short circuit between the foils and then the layers of materials are wound around on one another and then placed into an aluminum can. A sketch of a typical aluminum electrolytic capacitor is shown in figure (11).

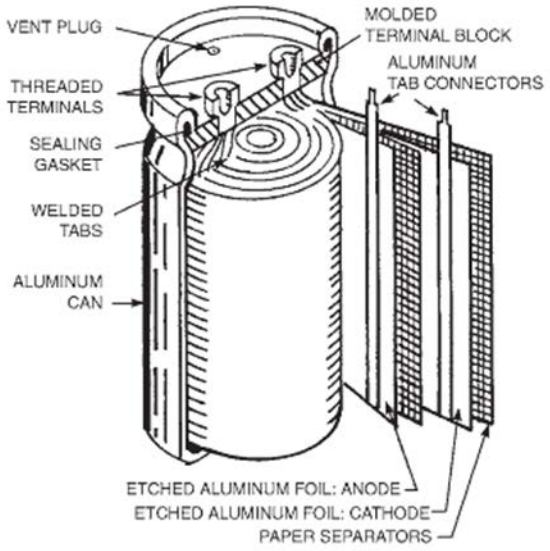

Fig. 11- Aluminum electrolytic capacitor [11].

However, while these capacitors offer high CV ratios and are low in cost, they exhibit high DC leakage and low insulation resistance and the fact that their performance and reliability strongly depend on the operation temperature. In principle, the lifetime of an aluminum electrolytic capacitor generally doubles for each 10 °C temperature reduction in the capacitor core. [12] The core is the hottest spot of the capacitor and approximately at the center of the capacitor. The evaluation of the core temperature is generally obtained by three factors; namely, the ambient temperature, the power dissipation in the capacitor, and the thermal resistance between the capacitor core and the ambient air [13].

The lifetime of capacitor is mainly established by the component temperature. Therefore it is critical to anticipate heating under operating conditions already in the early stage of development. This can be used in optimization of the electronics design with regards to selecting the most suitable type of capacitor.

Many manufacturers are trying to tabulate values of thermal resistances for the thermal core to case and core to air resistances [14]. Parler [15] and Huesgen [13] have developed more specific models by investigating numerous cooling techniques for large capacitors with screw and snap in terminals.

3.3 **Motivation and Objective**

Choosing the right capacitor has significant role for an application. It involves knowledge of different aspects of application environment, including thermal and electrical. [16] The life of an aluminum electrolytic capacitor varies exponentially with temperature, therefore the thermal modeling concept is substantial. [15]

To build a thermal model it is necessary to know the thermal parameters. These parameters are:

- thermal conductivities.
- thermal capacitances.

Basic analytical equations for heat conduction can be applied for the known geometries and commonly used materials (such as aluminum can and aluminum leads). The capacitor winding is a more complex part. This is composed of a cathode and an anode layer. These layers are separated by paper, impregnated by a liquid

electrolyte. The winding has very high anisotropic properties. This is influenced by much higher thermal resistance in radial than in axial direction. Also there are undefined properties like compression factor of the paper and material data of the electrolyte or the gaps between the winding and the can. Because of these latter factors, Parler [15] measured the thermal properties of the winding using a special test stand. Then he was able to employ these properties to a one-dimensional model. In his model the complex winding structure is represented by a thermal resistance in radial and in axial direction. Parler and Macomber later used these results to build a thermal network model. Their model consisted of seven resistive elements based on analytical equations [14].

However, the objective of this work is to investigate an analytical solution for the aluminum electrolytic capacitor by applying the general equation of energy conservation, and considering the independency of k by space and temperature and the heat generation due to the joule effect. Then, to compare the results to the FE-computer- solved results.

Modelling the heat transfer for capacitor can

During the course of the device functioning, the capacitor temperature reaches to a higher temperature than the environment temperature. And under steady state conditions, the heat power dissipated to the medium should be equal to the power generated by the capacitor according to the balance of energy.

$$P_{gen} = P_{th} \qquad [3.1]$$

The ways in which heat transfer mechanisms is being distributed around and inside the capacitor may include conduction, (free or forced) convection and radiation. In this case, the convective heat transfer is the mean to cool the capacitor from the can to the ambient. It is generally modelled as a surface effect that depends on fluid mechanics, medium temperature, heat and mass transfer properties such as density, specific heat and viscosity, geometry of device and direction of flow. Assuming the surface of the device is at a higher temperature than the environment by an amount ΔT, the power dissipated through the convection is given by

$$P_{conv} = h_{conv} A_s \Delta T \qquad [3.2]$$

where A_s is the surface area of the capacitor where the convection occurs. Similarly, radiation is also a surface effect. Its capability depends on material properties of the capacitor surface and the absolute temperature as well as the temperature difference between the can surface and the ambient. This is governed by Stefan-Boltzmann's law as

$$P_{conv} = \varepsilon\sigma\left(T_s^4 - T_\infty^4\right) = h_{rad} A_s \Delta T \qquad [3.3]$$

where ε is the radiation coefficient (emissivity). For an aluminum electrolytic capacitor that is covered with an isolating sleeve ε = 0.85 is a good approximation, while for bare capacitors ε = 0.4 [15].

At standard atmospheric pressure and temperature controlled, the medium would be air at values ranging from 20 to 30 °C. In electrical industry an approximate value of h is commonly used which is linked to velocity of cross flow air via the correlation:

$$h = 11\sqrt{(V + 0.25)/(0.25)} \qquad [3.4]$$

in units of $Wm^{-2}K^{-1}$. According to [15], above correlation lumps together all the effects of natural convection, forced convection and radiation processes. In the present analysis, although it does not take into account many other important factors for capacitor such as gravimetric orientation, the aspect ratio and the type of air flow laminar or turbulent, h is used as a known quantity being equal to 11 $Wm^{-2}K^{-1}$ by taking the velocity as 0 ms^{-1}. Thus, by means of equation (3.4), the defining energy balance is given as

$$W_i V = h A_s \Delta T \qquad [3.5]$$

A schematic diagram and nomenclature of a capacitor model is simply illustrated in figure (12), where all the surface of the capacitor is exposed to a convection environment characterized by h∞, T∞.

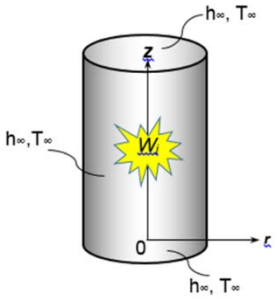

Fig. 12- Model of the capacitor under convection environment.

An electric circuit was set up in order to check the superficial temperature of the device under assigned convection heat transfer through ventilation as shown in figure (13) A few simplifications were made on the value of thermal conduction leading to the known physical quantities as dimensionless variables: Biot number in x and r directions. The analytical result, obtained as a series expansion, has the advantage of being correct and usable in a large range of devices, provided an adequate number of eigenvalues is employed.

Fig. 13- Test Setup.

3.4 **Analytical Solution**

When the exact steady solution is sought, the unsteady term of heat conduction equation on the r.h.s (right hand side) is zero. Therefore, the differential equation which governs the steady conduction of heat across a two dimensional solid (or fluid) in cylindrical coordinates [2], considering there is no angular variation, with z and r are the only spatial coordinates is

$$\frac{1}{r}\frac{\partial}{\partial r}\left(r\frac{\partial T}{\partial r}\right)+\frac{\partial^2 T}{\partial z^2}+\frac{W_i}{k}=0 \qquad [3.6]$$

where the body is assumed to be homogeneous, k is the material conductivity and W_i is the constant and uniformly distributed internal heat generation. In order to make the boundary conditions homogeneous, θ is defined as the spatial temperature distribution referred to the known ambient temperature T_∞. And only half of the capacitor length is considered since the problem is symmetrical in axial position z about z=L. In other words, the origin is replaced in the center of the cylindrical model and imposed an adiabatic condition at z=0.

If there were no heat generation, equation (3.6) would be solved through the separation of variables, since boundary conditions are homogeneous in terms of temperature difference with ambient medium. However, the volumetric power density W_i is the known term in the equation, thus we moved to investigate a solution which is given by superposition method as the sum of two effects θ_1 and θ_2, that obey to two different differential equations; namely, a steady state one-dimensional heat equation with power density and a partial second order differential equation, homogeneous in θ_2 with no heat generation as given below

$$\theta(r,z)=\theta_1(r)+\theta_2(r,z) \qquad [3.7]$$

where θ_1 is chosen as a function of only r-direction. As an alternative solution, it would also be possible to choose θ_1 as a function of only z-direction However, in present analysis the heat generation term is implemented to be absorbed in θ_1 which is a function of only r-direction. Therefore; corresponding equations are given in the following.

$$\theta_1(r) = \frac{1}{r}\frac{d}{dr}\left(r\frac{d\theta_1}{dr}\right) + \frac{W_i}{k} = 0 \qquad [3.8]$$

$$\theta_2(r,z) = \frac{1}{r}\frac{\partial}{\partial r}\left(r\frac{\partial\theta_2}{\partial r}\right) + \frac{\partial^2\theta_2}{\partial z^2} = 0 \qquad [3.9]$$

Then taking into account the symmetry of the cylinder at center r=0 and z=L, the boundary conditions which have to be satisfied are derived for the quarter of the cylinder model as

- b.c.1. $\left.\frac{d\theta_1(r)}{dr}\right|_{r=0} = 0$
- b.c.2. $\left.\frac{d\theta_1(r)}{dr}\right|_{r=a} = -\frac{h}{k}\theta_1(a)$
- b.c.3. $\left.\frac{\partial\theta_2(r,z)}{\partial r}\right|_{r=0,z} = 0$
- b.c.4 $\left.\frac{\partial\theta_2(r,z)}{\partial r}\right|_{r=a,z} = -\frac{h}{k}\theta_2(a,z)$
- b.c.5 $\left.\frac{\partial\theta_2(r,z)}{\partial z}\right|_{r,z=0} = 0$
- b.c.6. $\left.\frac{\partial\theta_2(r,z)}{\partial z}\right|_{r,z=L} = -\frac{h}{k}\left[\theta_1(r) + \theta_2(r,L)\right]$

The solution of equation (3.8) which is an ODE is straight forward, coupled with heat balance:

$$r\frac{d\theta_1}{dr} = \frac{W_i}{k}\frac{r^2}{2} + C_1 \qquad [3.10]$$

Applying the b.c. (1) into equation (3.10) yields that C_1 must be equal to 0. Then, again differentiating the equation gives

$$\theta_1(r) = \frac{W_i r^2}{4k} + C_2$$

In order to find the constant C_2, as mentioned above before, from energy balance we have:

$$W_i\left(\pi a^2 L\right) = h\Delta T\left(2\pi a L\right) \qquad [3.11]$$

By rearranging the above equation, the spatial surface temperature can be expressed as

$$\Delta T = \frac{W_i a}{2h} = \theta_{\text{surf}} \qquad [3.12]$$

Therefore, solution of θ_1 results in

$$\theta_1(r) = \frac{W_i a^2}{4k}(1 - \frac{r^2}{a^2}) + \frac{W_i a}{2h} \qquad [3.13]$$

Subsequently, equation (3.9), which is a Laplace's equation, is solved by utilizing separation of variables method. The existence of a product solution of two functions is assumed; namely, one a function of the z coordinate only and one a function of the radial coordinate only.

$$\theta_2(r,z) = R(r)Z(z) \qquad [3.14]$$

Then, this equation is superseded for θ_2 into equation (3.9) and the following result is obtained.

$$\frac{1}{r}\frac{\partial}{\partial r} r \frac{\partial\left[R(r)Z(z)\right]}{\partial r} + \frac{\partial^2\left[R(r)Z(z)\right]}{\partial z^2} \quad \Rightarrow \quad Z(z)\frac{1}{r}\frac{\partial}{\partial r} r \frac{\partial R(r)}{\partial r} + R(r)\frac{\partial^2 Z(z)}{\partial z^2} = 0 \qquad [3.15]$$

Each term of equation (3.15) is divided by R(r)Z(z) and each side is set equal to a constant that result in

$$\frac{R''(r)}{R(r)} + \frac{1}{r}\frac{R'(r)}{R(r)} + \frac{Z''(z)}{Z(z)} = 0 \quad \Rightarrow \quad \frac{R''(r)}{R(r)} + \frac{1}{r}\frac{R'(r)}{R(r)} = -\frac{Z''(z)}{Z(z)} = -\alpha^2 \qquad [3.16]$$

The sign of the separation constant is chosen $-\alpha^2$ since the homogenous boundary conditions are in the direction of r, such that eigenfunctions are obtained in this direction. Hence, the two ordinary differential equations in conjunction with their boundary conditions separately expressed as first order equations bring following solutions. Firstly, the solution for Z is given by hyperbolic functions as

$$Z''(z) - \alpha^2 Z(z) \quad \Rightarrow \quad Z(z) = C_1 \sinh\left(\alpha z\right) + C_2 \cosh\left(\alpha z\right) \qquad [3.17]$$

and the solution of R is expressible in terms of the general Bessel's equations as

$$r^2R^{''} + rR^{'} + \alpha^2 r^2 R = 0 \quad \Rightarrow \quad R(r) = C_3 J_0(\alpha r) + C_4 Y_0(\alpha r) \qquad [3.18]$$

Thereby, the general form of the solution for θ_2 becomes

$$\theta_2(r,z) = \left[C_1 \sinh(\alpha z) + C_2 \cosh(\alpha z)\right]\left[C_3 J_0(\alpha r) + C_4 Y_0(\alpha r)\right] \qquad [3.19]$$

The above set of ordinary differential equations in conjunction with the boundary conditions have to be satisfied. Firstly, the homogenous r boundary conditions are used in order to determine the eigenfunctions and the eigenvalues of the problem. Since all Y_n become $-\infty$ as r becomes zero; to keep the solution finite, b.c. (3) requires that $C_4 = 0$. The eigenfunctions of the problem become $J_0(\alpha_n a)$. And applying the convection b.c. (4) by use of the formulas for the derivative of J_0 yields following relationship

$$-\alpha J_1(\alpha a) C = -\frac{h}{k} J_0(\alpha a) \qquad [3.20]$$

which is the eigencondition to the problem and for convenient it may be rewritten as:

$$\frac{\alpha a}{Bi_a} = \frac{J_0(\alpha a)}{J_1(\alpha a)} \quad \Rightarrow \quad \frac{\lambda}{Bi_a} = \frac{J_0(\lambda)}{J_1(\lambda)} \qquad [3.21]$$

Where the Bi_a is the Biot number in the direction of r, equal to ha/k. Moreover, the roots of equation (3.21) give the eigenvalues and there are infinite number of real eigenvalues which satisfy the equation (3.21), as $\alpha_1 a$, $\alpha_2 a$, $\alpha_3 a$, ……. $\alpha_n a$, where $\alpha_n < \alpha_{n+1}$ (n = 1, 2, …) And graphically, all these values can be shown as intersections of the function $f(\lambda) = J_0(\lambda) * Bi_a - J_1(\lambda) / \lambda = 0$ with the λ-axis as shown in figure (14).

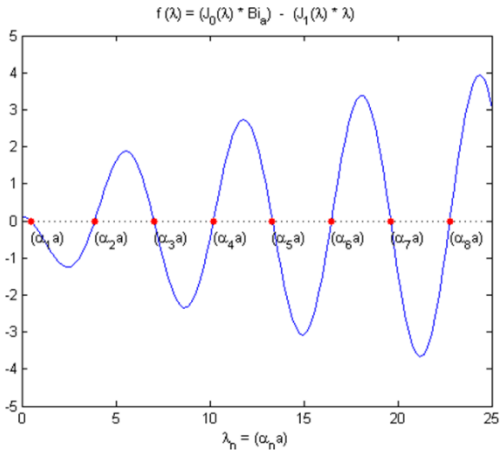

Fig. 14- Points of eigenvalues.

In traditional way, the acceptable values of these positive roots are indicated as the abscises of intersections of the graph of $J_0(\lambda)$ / $J_1(\lambda)$ with the graph of a straight line through the origin with a slope of λ / Bi_a as plotted in figure (15). These eigenvalues are computed with Matlab™ program.

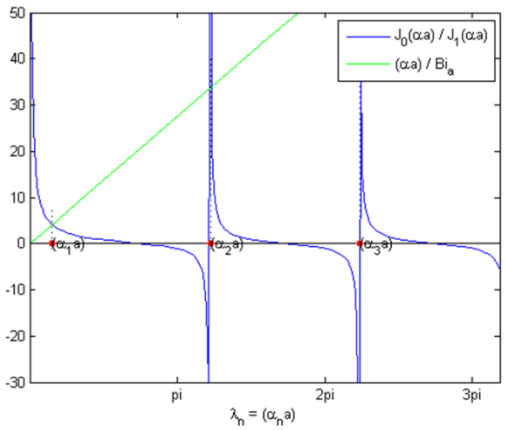

Fig. 15- Eigenvalues to the problem at intersections.

The properties of Bessel and trigonometric functions is used to cancel part of the two unknown constants and to solve the b.c. equations (first order ODEs) for which the roots (eigenvalues) are obtained. On the other hand, to satisfy the boundary condition (5) that is $\partial\theta_2 / \partial z = 0$, C_1 must be equal to 0. Hence, the product solution is rewritten as the sum of all eigenvalue solutions, namely, each multiplied by a different constant as following

$$\theta_2(r,z) = \sum_{n=1}^{\infty} C_n \cosh(\alpha_n z) J_0(\alpha_n r) \qquad [3.22]$$

We are now left with infinite functions $\theta_{2,n}$ unknown by a constant C_n, because they satisfy the three homogenous b.c.s. 3, 4 and 5 of the problem. Therefore, we will look for a series expansion that satisfies the remaining b.c. (6). Setting z = L in equation (3.22) gives the following equation for the non-homogenous boundary condition.

$$\left.\frac{\partial\theta_{2,n}}{\partial z}\right|_{r,z=L} = -\frac{h}{k}\left[\theta_1(r) + \sum\nolimits_n C_n \cosh(\alpha_n L) J_0(\alpha_n r)\right] \qquad [3.23]$$

Then, rearranging equation (3.23) results in

$$\sum C_n\left(\alpha_n \sinh(\alpha_n L)+\frac{h}{k}\cosh(\alpha_n L)\right)J_0(\alpha_n r)=-\frac{h}{k}\left[\theta_1(r)\right] \qquad [3.24]$$

A use of the orthogonality condition for the Bessel functions, which has a weighting function r, is now made to compute the remaining unknown C_n's. Namely, each side of equation (3.24) is multiplied by $rJ_0(\alpha_n r)$ and integrated over the r domain - which extends from a lower limit of zero to an upper limit of a – this gives the following result

$$\sum C_n\left(\alpha_n \sin(\alpha_n L)+\frac{h}{k}\cos(\alpha_n L)\right)\int_0^a rJ_0{}^2(\alpha_n r)dr=-\frac{h}{k}\left[\int_0^L \theta_1(r)rJ_0(\alpha_n r)dr\right] \qquad [3.25]$$

since after the rJ_0^2 integration kills off all terms in the series except for n=m. Therefore, C_n expansion coefficients become

$$C_n=\frac{-\frac{h}{k}\left[\int_0^a \theta_1(r)rJ_0(\alpha_n r)dr\right]}{\left[\alpha_n \sinh(\alpha_n L)+\frac{h}{k}\cosh(\alpha_n L)\right]\left[\frac{a^2}{2}\left(J_1{}^2(\alpha_n \mathrm{a})+J_0{}^2(\alpha_n \mathrm{a})\right)\right]} \qquad [3.26]$$

Upon evaluating the integration of θ_1 in the numerator and introducing the result the unknown values of C_n expansion coefficient is expressed as

$$C_n=\frac{\left(\frac{W_i \mathrm{a}^2}{2h_\infty}\frac{J_1(\alpha_n \mathrm{a})}{\alpha_n}\right)-\left(\frac{W_i \mathrm{a}^2}{2k\alpha_n^2}\right)\left(J_0(\alpha_n \mathrm{a})-\frac{2J_1(\alpha_n \mathrm{a})}{(\alpha_n \mathrm{a})}\right)}{\left[\alpha_n \sinh(\alpha_n L)+\frac{h_\infty}{k}\cosh(\alpha_n L)\right]\frac{a^2}{2}\left(J_1{}^2(\alpha_n \mathrm{a})+J_0{}^2(\alpha_n \mathrm{a})\right)} \qquad [3.27]$$

Therefore, the solution of C_n eventually are substituted into equation (3.22) and then the final result of the temperature distribution for cylindrical capacitor is obtained as

$$T-T_\infty=\theta=\frac{W_i a^2}{4k}\left(1-\frac{r^2}{a^2}\right)+\frac{W_i a}{2h}+\sum_{n=1}^{\infty}C_n \cosh(\alpha_n z)J_0(\alpha_n r) \qquad [3.28]$$

3.4.1 Results and discussions

The above final expressions for $T(r, z)$, which may even easily be inserted into a palmar calculator that has "math" solvers, have been implemented in Matlab™ ambient. Since the analytical solution is the summation of an infinite series, only a finite number of terms are taken into account while obtaining the analytical solution after checking the effect of number of terms on the result. In other words, the equations are evaluated until the change in the temperature is less than the desired tolerance. And, it is found that the solution converges with more than 5 terms and it does not change appreciably when an additional number of terms is used.

The representation of these analytical results are given in the following figures. Firstly, θ_1 and θ_2 are plotted within Matlab™ as shown independently in figure (16) to visualize that how their summation together with ambient temperature form the final result of the temperature distribution. And in figure (17), the 3D-view of $T(r, z)$ together with its surface-map onto base is given to give a good qualitative overview of the full space temperature distribution for the capacitor model.

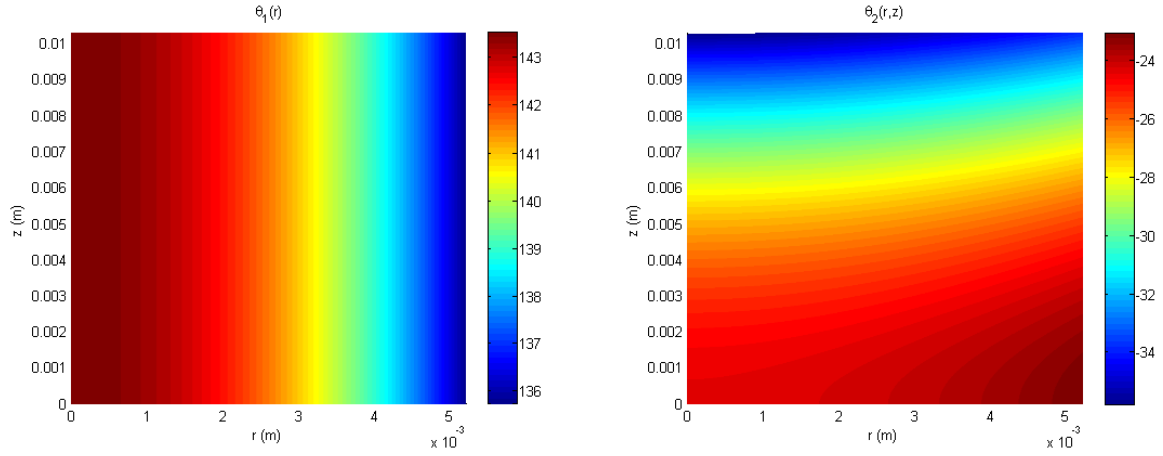

Fig. 16- 2D plots of θ_1 (left) and θ_2 (right).

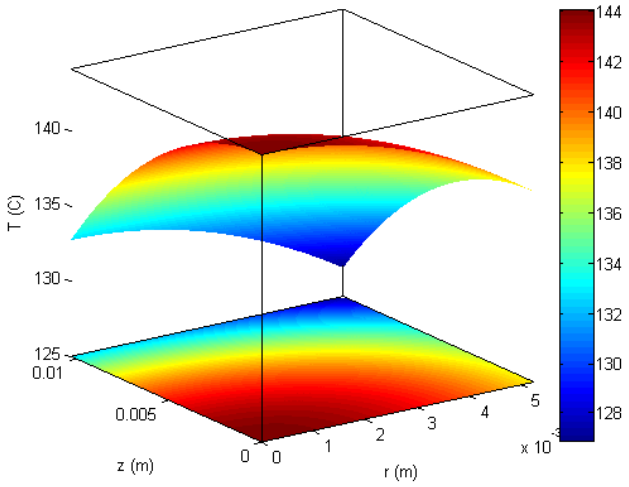

Fig. 17- 3D plot of the analytical temperature distribution as a function of distance in r-direction (m) and in z-direction (m) in a cylindrical capacitor model.

3.5 **Finite element method solution**

Figure (18) presents the temperature contours in the modeled cylindrical capacitor under same conditions with an uniformal heat generation an amount of 574234 [W/m^3].

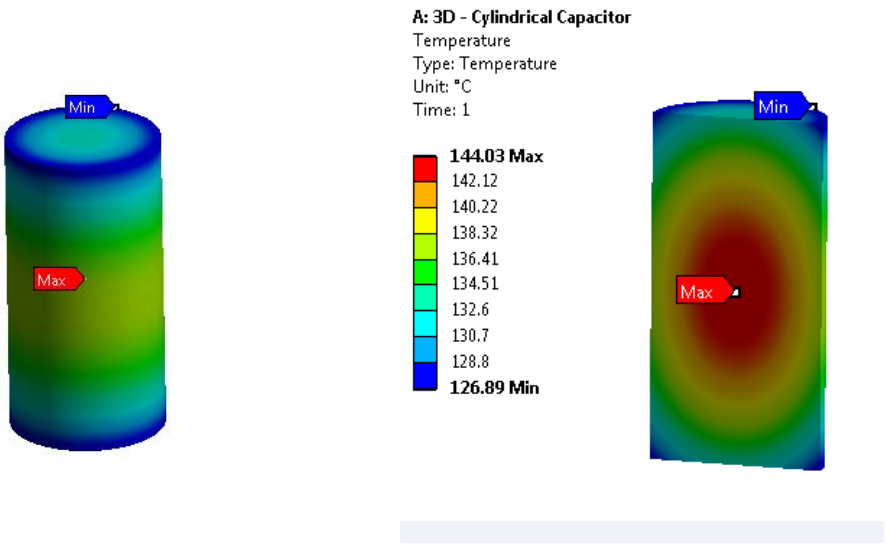

Fig. 18- Temperature contours in a cylindrical capacitor model.

3.6 Comparison of results of the analytical method and the FEM method

Figure (19) and (20) presents the comparison between analytical and finite element analysis. The temperature profiles perfectly matches between these solution through either r or z direction.

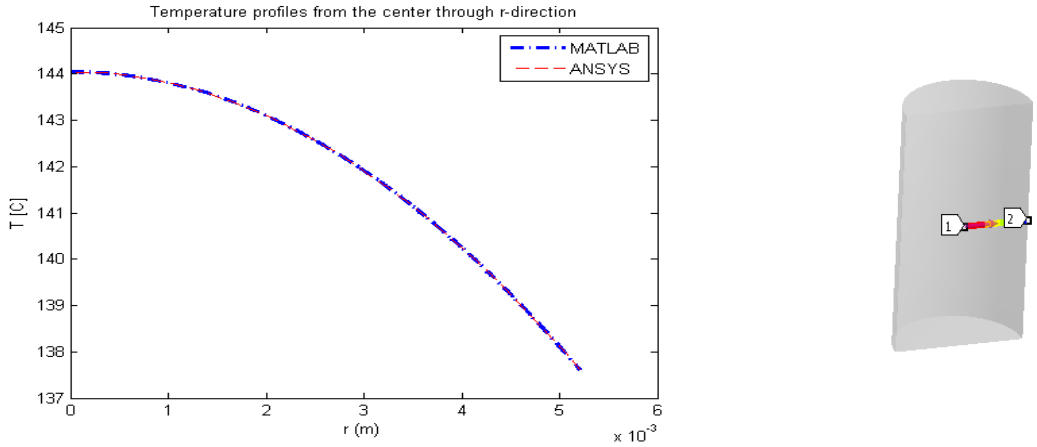

Fig. 19- Comparison of temperature variation between analytical and FEM results through r – direction.

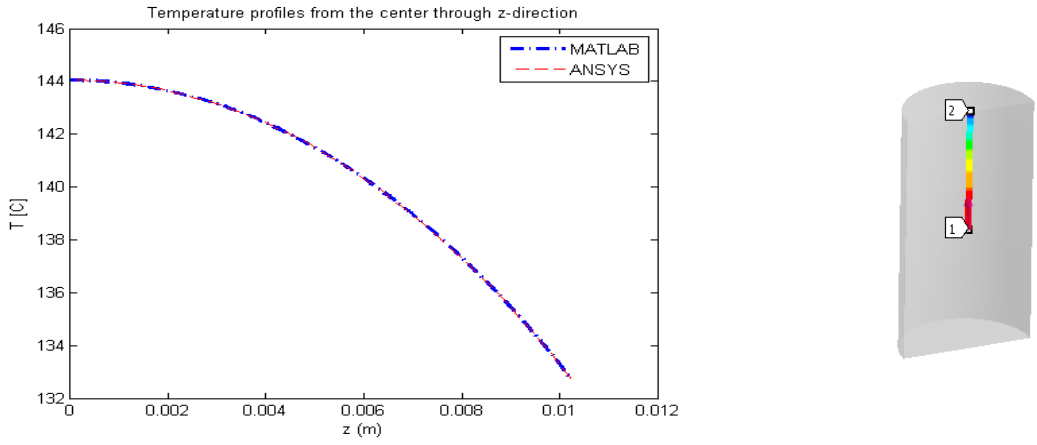

Fig. 20- Comparison of temperature variation between analytical and FEM results through z – direction.

3.7 **Conclusion**

The present work found an analytical solution for a cylindrical capacitor model. The analytical solution of the heat transfer partial differential equations presented in this section appears in the form of the sum of the effects. The results are obtained in terms of a series expansion solution involving Bessel functions based on the principle of superposition and separation of variables.

And then, a comparison between the analytical results and the numerical results obtained through a FEA package, ANSYS™. The comparison shows that they are in excellent agreement.

Thus, the analytical solution is valuable because it can be even obtained by simple math solvers and palmar calculators and is a mean of validating the numerical schemes or vice versa when experimental data of the engineering problem are available.

Chapter 4

A tinplate can filled with beef homogenate under thermal sterilization

4.1 Basic concepts of heat transfer in Food Processing Industry

A myriad of food processing operations involve the transfer of heat, such as cooking, roasting, sterilization, chilling, freezing. Therefore, a good understanding of the principles that govern heat transfer becomes an essential subject also in the food processing industry.

Thermal processing of food products is done by either heating or cooling. It's objective is to produce a product which is stable and could be stored for longer periods. Such product should be free from pathogenic organisms, which cause food spoilage. [17] Various enzymes and microorganisms are interacting with food and making it unsuitable for humans. In order to prevent it, these enzymes and microorganisms should be destroyed or partially or totally inhibited and food should be stored in proper packaging. The outcome of heat treatment correlates with time and temperature. Generally, the effect is greater with increase of temperature and time. There are various techniques of food preservation by heat treatment. These includes:

- Sterilization; Pasteurization; Drying; Cooking; Laundering.

Sterilization by heat is achieved by exposing food to temperature which normally surpass 100°C for a period of time ample enough to inhibit enzymes and various forms of microorganisms in sealed containers. To obtain a commercially sterile product conditions applied to product should be specified. The success is granted only by applying heat for a certain period of time at the certain temperatures, under determined conditions [18]. However, this technique does not grant the long-term

conservation by itself. In everyday conditions food is affected by subsequent contamination by environmental microorganisms. Therefore the food container most also be sterilized. The sterilization of both, food and container, can be achieved in the following two ways:

- Appertization.
- Aseptic packaging.

Appertization is a technique when container and its content is sterilized simultaneously. Aseptic packaging is when container and its content are sterilized separately. When designing thermal food process operations two criteria outstand. The temperature in the slowest heating zone (SHZ) and the thermal center of the food during the process are essential. This temperature is measured using thermocouples [19]. This allows the possibility to evaluate the effect of the thermal treatment on the microbiological and sensory quality using well-established methods. Traditional methods of temperature measurements and quantitative microbiological and food quality analyses are very time consuming. Therefore mathematical models and simulation software can be an advantageous alternative. [20]. Heat transfer modes can be classified when considering sterilization of canned food. These types include:

- Conduction through solid foods.
- Convection through liquid foods, especially those having low viscosity. This convection can be natural or forced, depending on whether the motion of fluid is induced artificially or not.
- Combined convection-conduction through liquid food with high viscosity.

However, commonly in the applications conduction is assumed as the only heat transfer mode which can only be used for solid food. This is due to the relative simplicity of analytical and numerical solutions. In the case, when heat transfer is only controlled by conduction, then during the heating process the so-called SHZ remains at the geometric center of the can [19].

Most of the thermally preserved products are in metal containers (cans) while others are packed in glass jars or plastic or aluminum/plastic laminated pouches. Most metal containers are cans or “tins” produced from tinplate and they have usually a

cylindrical shape. In this study, it is also considered a tinplate can filled with beef meat which has a cylindrical shape as shown in figure (21).

Fig. 21- Tinplate can filled with beef homogenate.

The relevant thermal and physical properties of foods for mathematical modelling of conduction heat transfer are thermal conductivity (k), specific heat (c_p) and density (ϱ). These thermo-physical properties may be temperature dependent which make the problem non-linear. The values of these parameters are assumed to be constant in the analytical solution for the sake of the simplicity of the problem. Besides, they are considered as a mild function of temperature in the finite element method solution.

4.1.1 **Motivation and Objective**

Sterilization of a tinplate can filled with beef homogenate was theoretically and experimentally modeled and the finite element method was applied to the calculation of temperature profiles under unsteady heating and cooling stages [21]. The objective of this chapter was to obtain an analytical solution for sterilization process of the can in the heating stages.

The dimensions for the cylindrical can are taken to be a radius of a = 36 mm and a height of 2c = 104 mm and where the can is heated from all sides at 123°C with an uniform initial temperature of 21.5°C.

4.2 **Analytical Solution**

Generally, in thermal food processes the heat generation is assumed to be zero since the chemical reactions do not generate large amounts of heat except those involve volumetric heating such as microwave heating. In present study of the case of tinplate can filled with beef under sterilization there is also no volumetric heat generation and it is decoupled from the differential equation and the case is

unsteady. Therefore, the general differential equation which governs the unsteady-conduction of heat across a two dimensional solid (or fluid) in cylindrical coordinates is written as the following equation [2],

$$\frac{1}{r}\frac{\partial}{\partial r}\left(r\frac{\partial T}{\partial r}\right)+\frac{\partial^2 T}{\partial z^2}=\frac{1}{a_t}\frac{\partial T}{\partial t} \qquad [4.1]$$

where the heat transfer is assumed to be significant in radial (r) and longitudinal (z) directions while it is neglected in angular direction due to symmetry boundary conditions, and the thermo-physical parameters ϱ, c and k are assumed to be constant for the sake of simplicity in the analytical solution.

Usually, in canning processes, the convection boundary condition at the outer surface and symmetry boundary condition in the centreline are preferred. In this study it is also proceeded that the tinplate can loses heat from its outer surface according to Newton's law of cooling. Since the problem is symmetrical in axial position z about z=c, only half of the tin can length is considered. In other words, the origin is replaced in the center of the cylinder model and imposed an adiabatic condition at z=0 as it is shown in figure (22).

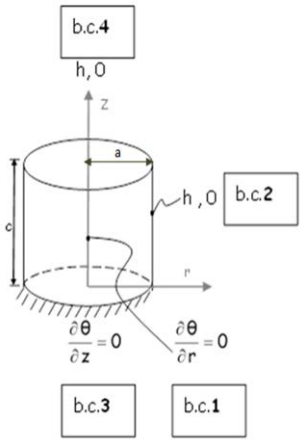

Fig. 22- The model of can with corresponding boundary conditions.

In order to make the boundary conditions homogeneous, first, θ is defined as the spatial temperature distribution referred to the known ambient temperature T_∞. Additionally, initial temperature is defined as being equal to $\theta_i = T_{initial} - T_\infty$. Therefore, the initial condition and the boundary conditions which are to be satisfied are given as

- b.c.1. $\left.\frac{\partial \theta(r,z,t)}{\partial r}\right|_{r=0,z,t} = 0$
- b.c.2. $\left.\frac{\partial \theta(r,z,t)}{\partial r}\right|_{r=a,z,t} = -\frac{h}{k}\theta(a,z,t)$
- b.c.3. $\left.\frac{\partial \theta(r,z,t)}{\partial z}\right|_{r,z=0,t} = 0$
- b.c.4. $\left.\frac{\partial \theta(r,z,t)}{\partial z}\right|_{r,z=c,t} = -\frac{h}{k}\theta(r,c,t)$
- i.c. $\theta(r,z,0) = \theta_i$

Under all these considerations, a solution that is the product of three functions has been become possible in the form of the separation of variables namely; R(r) is a function of the radial coordinate only, Z(z) is a function of the z coordinate only and τ(t) is a function of the time only. Thus, by employing this product solution, the general solution is written as

$$\theta\left(r,z,t\right) = R\left(r\right)\cdot Z\left(z\right)\cdot \tau\left(t\right) \qquad [4.2]$$

This equation is superseded for θ into partial differential equation (4.1) and the following result is obtained.

$$Z(z)\tau\left(t\right)\frac{1}{r}\frac{\partial}{\partial r}r\frac{\partial R(r)}{\partial r} + R(r)\tau\left(t\right)\frac{\partial^2 Z(z)}{\partial z^2} = \frac{R(r)Z(z)}{a_t}\,\frac{\partial \tau\left(t\right)}{\partial t} \qquad [4.3]$$

Equation (4.3) is then divided through by the product R(r)Z(z)τ(t) solution, which yields

$$\frac{R^{''}}{R} + \frac{1}{r}\frac{R^{'}}{R} + \frac{Z^{''}}{Z} = \frac{1}{a_t}\frac{\tau^{'}}{\tau} \qquad [4.4]$$

The separation constant is set for the left hand side terms to be equal to respectively $-\alpha^2$ and $-\beta^2$ and for the right hand side term to be equal to $-(\alpha^2 + \beta^2)$. These yield three ordinary differential equations to solve as given with the following equations.

$$\frac{R^{''}}{R} + \frac{1}{r}\frac{R^{'}}{R} = -\alpha^2, \quad \frac{Z^{''}}{Z} = -\beta^2, \quad \frac{1}{a_t}\frac{\tau^{'}}{\tau} = -\left(\alpha^2 + \beta^2\right) \qquad [4.5]$$

These set of ordinary differential equations in conjunction with their boundary conditions expressed as first order equations bring following solutions. Firstly, the solution for R in r is given by the following form:

$$r^2R'' + rR' + \alpha^2 r^2 R = 0 \quad \Rightarrow \quad R(r) = C_1 J_0(\alpha r) + C_2 Y_0(\alpha r) \qquad [4.6]$$

Where J_0 and Y_0, are the known Bessel functions of the first and second kind with zero order [22]. In this equation coefficient C_2 is eliminated by applying b.c. (1), since all Y_n become -∞ as r becomes zero; therefore to keep the solution finite, it is required that $C_2 = 0$. Applying the convection b.c. (2) by use of the formulas for the derivative of J_0 as $dJ_0(r)dr = -J_1(r)$ provides the following needed eigenvalue relationship.

$$-C_1 \alpha J_1(\alpha a) = -\frac{h}{k} C_1 J_0(\alpha a) \qquad [4.7]$$

which is the eigencondition to that problem and for convenient it may be written as:

$$\frac{J_1(\alpha a)}{J_0(\alpha a)} = \frac{Bi_a}{(\alpha a)} \quad \Rightarrow \quad J_1(\lambda) = \frac{Bi_a}{(\lambda)} J_0(\lambda) \qquad [4.8]$$

where Bi_a is the Biot number in the direction of r and is equal to ha / k. The graph of these functions' behaviors are as shown in figure (23).

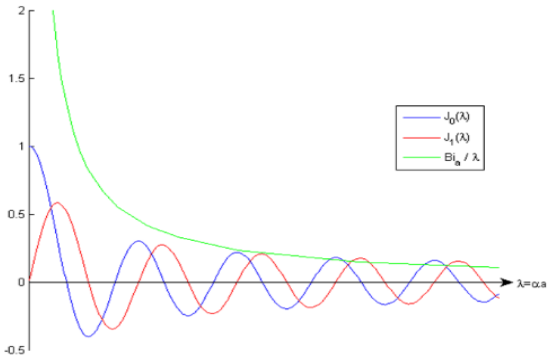

Fig. 23- The representation of behaviors of the related functions.

Moreover, the roots of equation (4.8) give the eigenvalues and there are infinite number of real eigenvalues as $\alpha_1 a$, $\alpha_2 a$, $\alpha_3 a$, …. $\alpha_n a$. And graphically, all these values can be shown as intersections of the graph of $J_0(\lambda) / J_1(\lambda)$ with the graph of a straight line through the origin with a slope of λ / Bi_a as plotted in figure (24).

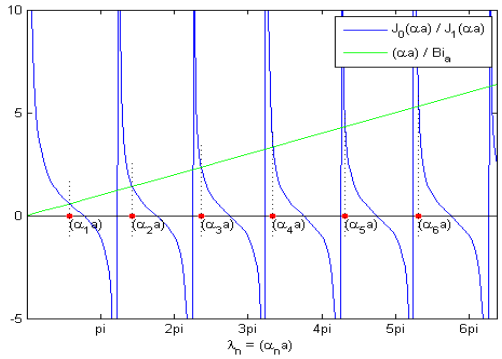

Fig. 24- Eigenvalues of the problem.

On the other hand, the general solution of the second term of equation (4.2) in z-direction is expressed as:

$$Z''(z)+\beta^2 Z(z) \quad \Rightarrow \quad Z(z)=C_3\sin(\beta z)+C_4\cos(\beta z) \qquad [4.9]$$

In this equation the coefficient C_3 is easily eliminated by the use of b.c.(3), $\partial Z/\partial z=0$ in order to satisfy the condition, namely, $\beta C_3\cos(\beta z)-\beta C_4\sin(\beta z)=0$, C_3 must be equal to 0. Then, the following needed eigenvalue relationship is obtained by applying the convection b.c (4).

$$-C_4\beta\sin(\beta c)=-\frac{h}{k}C_4\cos(\beta c) \qquad [4.10]$$

which is the another eigencondition needed for this problem and this can be written as the following equations in order to obtain a transcendental equation for β.

$$tg(\beta c)=\frac{Bi_c}{\beta c} \quad \text{or} \quad \cot(\lambda)=\frac{\beta c}{Bi_c} \qquad [4.11]$$

where Bi_c is, the Biot number in the direction of z, equal to hc / k. Here the infinite roots which satisfy the equation (4.11) are $\beta_1 a$, $\beta_2 a$, $\beta_3 a$, ……. $\beta_m a$, where $\beta_m < \beta_{m+1}$ (m = 1, 2, ...); and the acceptable values of these positive roots are indicated as the intersections of the graph of the cot(λ) with the graph of a straight line through the origin with a slope of $\beta_m c / Bi_c$ as plotted in figure (25).

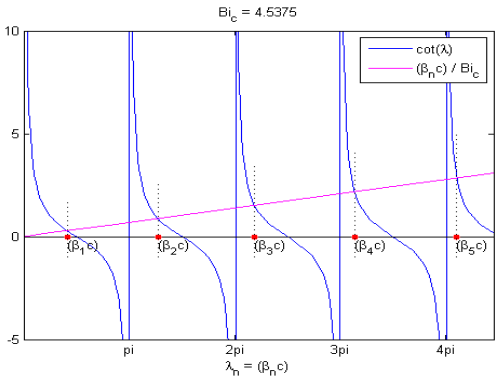

Fig. 25- Eigenvalues of the problem.

Here the values of λ_m, similar to the previous eigenvalues for J_0, are not evenly spaced and have to be found by numerical solutions. As the integer m increases, these values of λ_m will increase and as a result of this the intersections will come closer to an integer value of π while the cotangent term goes to infinity.

Finally, the general solution of equation of the third in t is obtained as

$$\tau'(t)+\left(\alpha_n^{\,2}+\beta_m^{\,2}\right)a_t\tau(t)=0 \quad \Rightarrow \quad \tau(t)=\exp[-\left(\alpha_n^{\,2}+\beta_m^{\,2}\right)a_t\,t] \qquad [4.12]$$

Since there are infinite number of terms for both n and m, the solution is summed over all n's and m's- a double summation. Thus, the product solution with the component solutions for $\theta(r,z,t) = R(r)Z(z)\tau(t)$ is expressed as:

$$\theta(r,z,t)=\sum_{n=1}^{\infty}\sum_{m=1}^{\infty}C_{nm}J_0\left(\alpha_n r\right)\cos\left(\beta_m z\right)\exp[-\left(\alpha_n^{\,2}+\beta_m^{\,2}\right)a_t\,t] \qquad [4.13]$$

There are an infinite series of roots in r and z, respectively the initial condition θ_i is then applied and is assumed that is equal to a series of functions with unknown C_{nm}.

$$\theta_i=\sum_{n=1}^{\infty}\sum_{m=1}^{\infty}C_{nm}J_0\left(\alpha r\right)\cos\left(\beta z\right) \qquad [4.14]$$

For the above equation it is made a use of the orthogonality properties of Bessel functions and cos functions with respect to the weighting factor r over the finite interval 0, a and 0, c. It is done by multiplying both sides of equation by $J(\alpha_n r)*r$ and $\cos(\beta_m z)$, and integrating the result over the said interval with the assumption that

the integral of the infinite sum is equivalent to the sum of integrals. Therefore equation (4.14) can be rewritten as following:

$$\int_0^a \theta_i\, r\, J_0\left(\alpha_n r\right) dr \int_0^c \cos\left(\beta_m z\right) dz = C_{nm} \int_0^a r\, J_0{}^2\left(\alpha_n r\right) dr \int_0^c \cos^2\left(\beta_m z\right) dz$$

Making the integrals for θ_i, which is constant and equal to T_i-T_∞

$$\theta_i \frac{\mathrm{a}}{\alpha_n} J_1\left(\alpha_n \mathrm{a}\right) \frac{\sin\left(\beta_m z\right)}{\beta_m} = C_{nm} \frac{a^2}{2}\left[J_1{}^2\left(\alpha_n \mathrm{a}\right) + J_0{}^2\left(\alpha_n \mathrm{a}\right)\right]\left[\frac{c}{2} + \frac{\cos\left(\beta_m c\right)}{2\beta_m}\sin\left(\beta_m c\right)\right]$$

After rearranging above equation results in:

$$C_{nm} = \theta_i C_n C_m = \theta_i \frac{2\mathrm{a} J_1\left(\alpha_n \mathrm{a}\right)}{\alpha_n \mathrm{a}^2\left[J_1{}^2\left(\alpha_n \mathrm{a}\right) + J_0{}^2\left(\alpha_n \mathrm{a}\right)\right]} \frac{2\sin\left(\beta_m c\right)}{\beta_m\left[\frac{c}{2} + \frac{\cos\left(\beta_m c\right)}{2\beta_m}\sin\left(\beta_m c\right)\right]} \qquad [4.15]$$

Hence, equation (4.15) gives following relationship for the constants:

$$C_n = \frac{2\ Bi_{\mathrm{a}}}{\left(Bi_{\mathrm{a}}{}^2 + \lambda_n{}^2\right) J_0\left(\lambda_n\right)} \quad \text{and} \quad C_m = \frac{2\sin\left(\beta_m c\right)}{\beta_m c + \cos\left(\beta_m c\right)\sin\left(\beta_m c\right)} \qquad [4.16]$$

Introducing these values into equation (4.14) the final solution in dimensionless form is obtained as:

$$\frac{\theta\left(r,z,t\right)}{\theta_i} = 2\,Bi_a \sum_{n=1}^{\infty} \frac{J_0\left(\lambda_n \frac{r}{a}\right) e^{-\lambda_n{}^2 Fo_a}}{\left(\lambda_n{}^2 + Bi_a{}^2\right) J_0\left(\lambda_n\right)} \bullet 2 \sum_{m=1}^{\infty} \frac{\sin\left(\beta_m c\right)\cos\left(\beta_m z\right) e^{-\beta_m{}^2 a_t t}}{\beta_m c + \sin\left(\beta_m c\right)\cos\left(\beta_m c\right)} \qquad [4.17]$$

Where; $Fo_{\mathrm{a}} = a_t / \mathrm{a}^2 t$ (Fourier Number) and $\alpha_n \mathrm{a} = \lambda_n$

4.2.1 **Results and discussions**

The representation of the analytical solutions are given in the following figures. By using the exact analytical solutions listed in this section and implemented in Matlab ambient, 3D plots of temperature per unit length and time are derived. In detail, the temperature contours of the analytical solution as a function of radial distance and

time is shown in figure (26) (a) and (b), respectively, while as a function of longitudinal distance is shown in figure 27 (a) and (b).

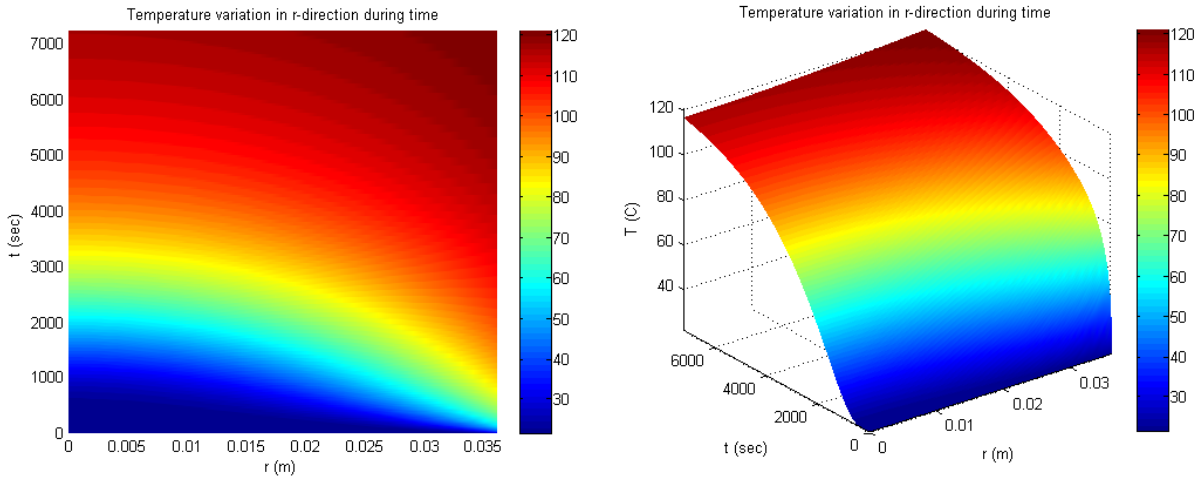

(a) (b)

Fig. 26- 2D and 3D plot of the analytical temperature distribution as a function of distance in r-direction (m) and time (s) for the cylindrical tinplate can model.

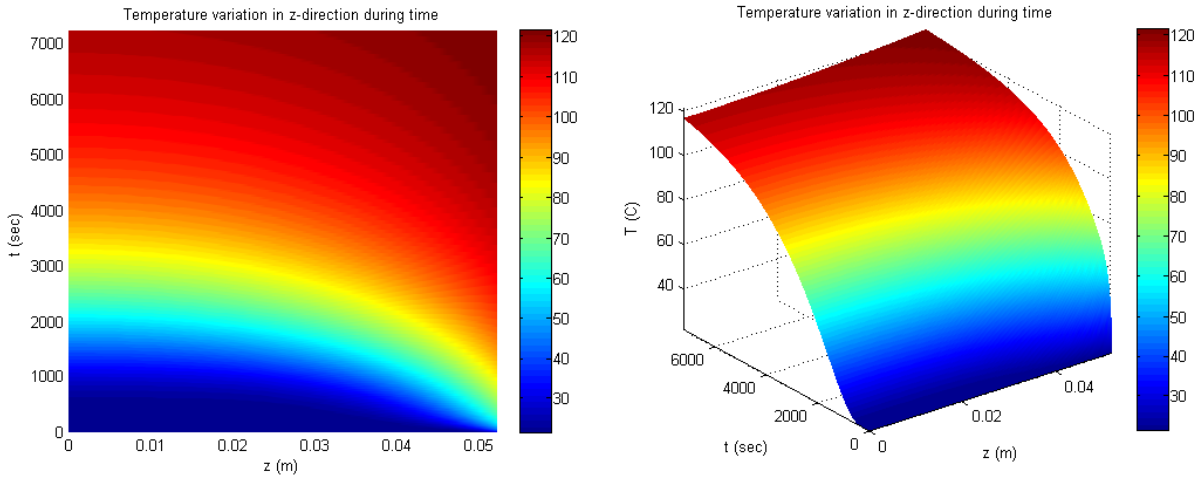

(a) (b)

Fig. 27- 2D and 3D plot of the analytical temperature distribution as a function of distance in z-direction (m) and time (s) for the cylindrical tinplate can model.

And figure (28) presents the plot of temperature distribution at the time of 7200 secs.

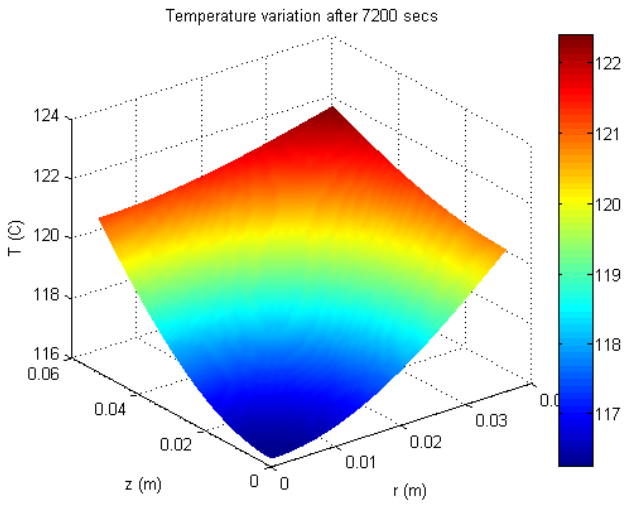

Fig. 28- 3D plot of the analytical temperature distribution as a function of distance in z-direction (m) and r-direction after 7200 seconds for the cylindrical tinplate can model.

4.3 **FEM Analysis**

A finite element model has been made for the purpose of making a comparison against to the analytical solution. Its dimensions are the same of the actual tin plate can that used in the analytical model but instead of 2D, in the finite element method it is modeled as a 3D. In the software Ansys™ Design Modeler Graphic user interface (GUI), it was built a 3D solid cylinder of radius r=0.036 (m) and of height z=0.104 (m). Again all the faces of the solid cylinder are considered to be subjected to convective conditions where the convective heat transfer coefficients on faces are equal and have values of 50 W/m²°C while the ambient temperature is 123 °C.

In transient analysis, in addition to the thermal conductivity, density and specific heat are specified hence the program calculates the heat storage characteristics of each element and then combines them in the specific heat matrix, which is denoted by C in equation (4.20).

Unlike the analytical solution, the temperature dependent both thermal conductivity and specific heat of the material are taken into account in the finite element analysis. The conductivity of the material is given as a mild function of temperature and isotropy is given, as shown in the figure (29). According to analysis of [21], the thermal conductivity of the material is expressed by the following empirical equation in the range of 40 - 123 (°C), while it stays constant between 20 and 40 (°C).

$$k = 0.573 \cdot [1 + 3.7 \cdot 10^{-4}(\mathrm{T} - 40)] \quad [\mathrm{W/m\,^{o}C}] \qquad [4.18]$$

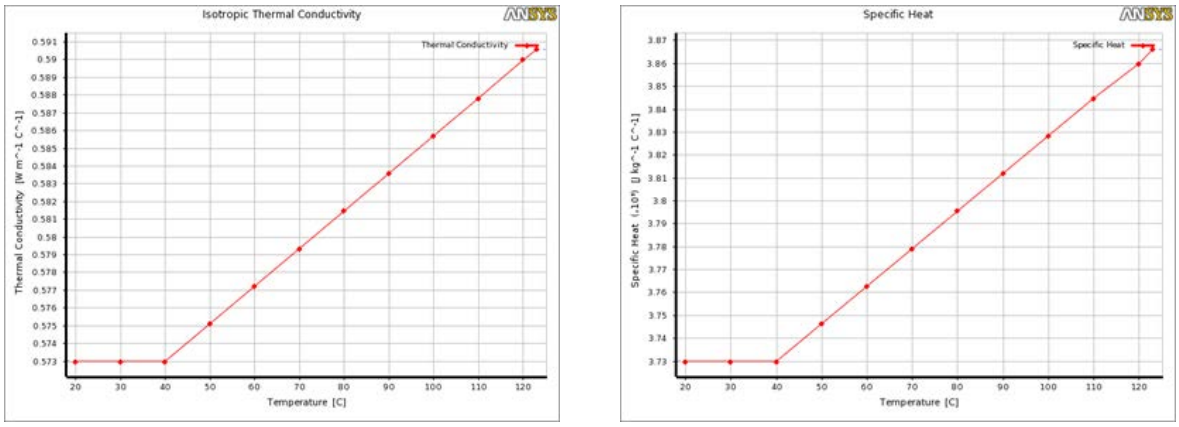

(a) (b)

Fig. 29- Thermal conductivity and specific heat as a mild function of temperature for the tinplate can.

And similarly, the specific heat is given as a function of temperature in the range of 40 -123 (°C) which is given in the equation (4.19), while it is constant and have a value of 3730 (j/kg°C) between 20 and 40 (°C).

$$c_p(40 - 123^{o}) = \mathrm{c}_p(20 - 40^{o})[1 + 4.4 \cdot 10^{-4}(\mathrm{T} - 40)] \quad [\mathrm{j/g\,^{o}C}] \qquad [4.19]$$

And finally density is given, as a constant property, being equal to 1060 (kg/m^3). Then, the cylindrical model is meshed using the three dimensional thermal solid element, SOLID90, which has 20 nodes with a single degree of freedom. The 20-nodes elements have compatible temperature shapes and are well suited to model curved boundaries. In addition to SOLID90, a three dimensional thermal surface effect element SURF152 is used by overlaying it onto the faces of the thermal solid elements for the consideration of the convection effects on the model's surface. Fig.11(b) shows the meshes generated for the present simulation. The applied model consists of 14866 nodes and a total number of 3268 elements as shown in the figure (30).

(a) (b)

Fig. 30- (a) Convectional boundary condition applied on the surfaces of model
(b) Shows the 3D model meshed

Since this case is a non-linear transient system, corresponding finite element equation expressing the thermal analysis, which ANSYS™ uses, can be written in matrix form as following:

$$\left[\left[C(T)\right]\right]\left\{\dot{T}\right\}+\left[K\right]\left\{T\right\}=\left\{Q(T,t)\right\} \qquad [4.20]$$

where C denotes the specific heat matrix.

Non-linear solutions in ANSYS™ / Mechanical are fundamentally based on the full Newton-Raphson iteration procedure [23]. Since, the thermal conductivity and the specific heat nonlinearities are given as a mild function of temperature in the current analysis, instead of full, a Quasi Newton-Raphson algorithm was used. That was speeded up the solution time significantly.

A thermal load of convection was applied all the surfaces of the solid cylinder as After all these proceedings, the transient thermal heat transfer finite element analysis was performed by taking the initial temperature 21.5 °C, as same as in the analytical solution. The load time step is again considered as 7200 seconds whereas the used minimum time step is 1e-03 and the maximum time step is 50 seconds.

The following figure (31) shows the temperature distribution in the solid cylinder model after 7200 seconds. As expected, the aliment cake is warmer near the surfaces due to the convection and the coolest point is the center of the solid cylinder.

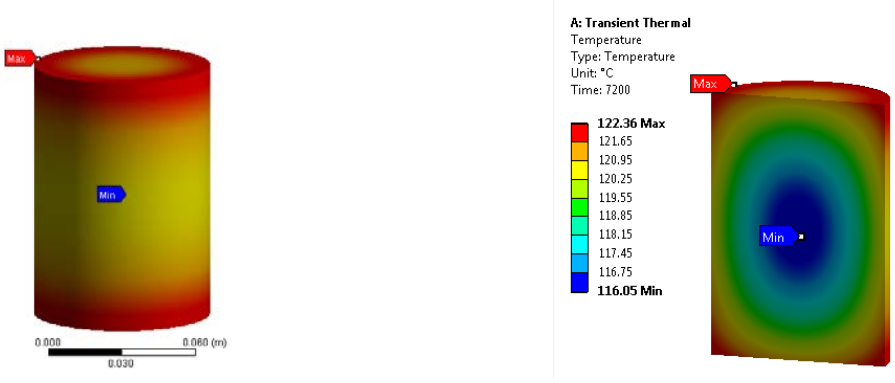

Fig. 31- FEM surface and mid – plane plots of contours of temperature in a tinplate can at the end of 7200 seconds with a rainbow representation.

4.3.1 **Results and the verification of the FEM analysis**

In order to check the validation of the results, two considerations has been analyzed. First is the accuracy of the results with the refined mesh. In other words, if the results converge when the mesh is refined. Therefore, a new mesh was made with a total number of 106513 nodes and 24928 elements.

To make a comparison of the results between refined mesh and previous one, temperature as a function of radial distance from the middle of the cylinder is plotted. As it is seen from the plot below, the FEA solutions for both meshes match very closely. Additionally, the finite element solution converges very quickly. In the figures below (32) and (32) there are two plotted lines; however, only one is visible since the variation is very minute. Hence this figure approves the good agreement between the used mesh and the refined mesh.

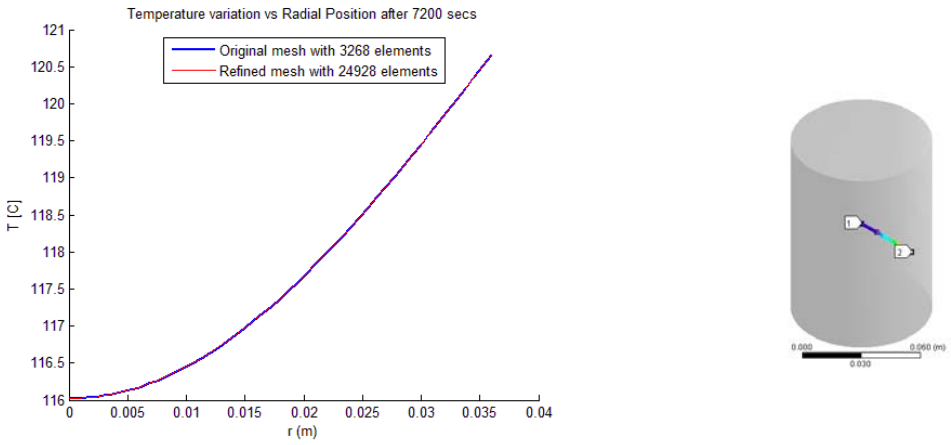

Fig. 32- Temperature variation vs Radial position after 7200 secs.

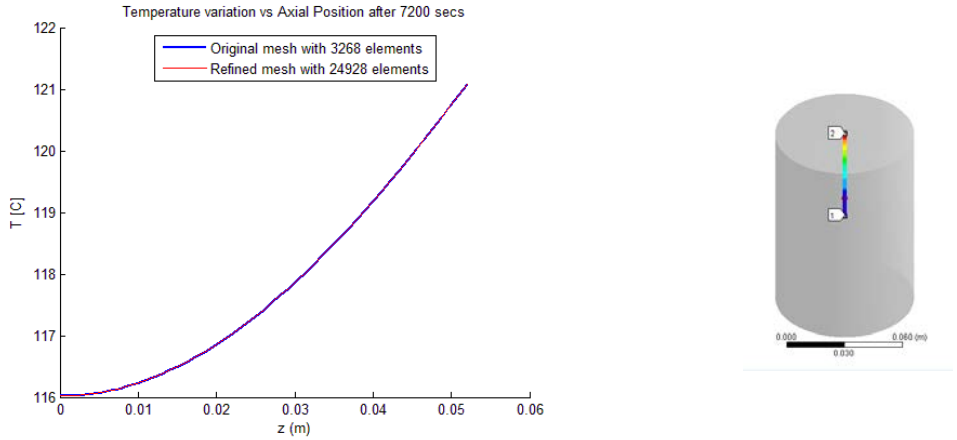

Fig. 33- Temperature variation vs Axial position after 7200 secs.

On the other hand, to check the validity of the FEA results, as much as refining mesh is important for obtaining accurate results, time is also considered as a second refinement factor that it may affect the solution. To do that, the number of time steps were altered and their temperature time history at the point of r=0.019 and z=0.027 (m) are plotted. As it is seen from the figure (34) when max time steps are enlarged, the results are changing significantly. Therefore the max time step as 50 seconds used in the analysis is enough to getting accurate results, with keeping on mind the costs of the analysis.

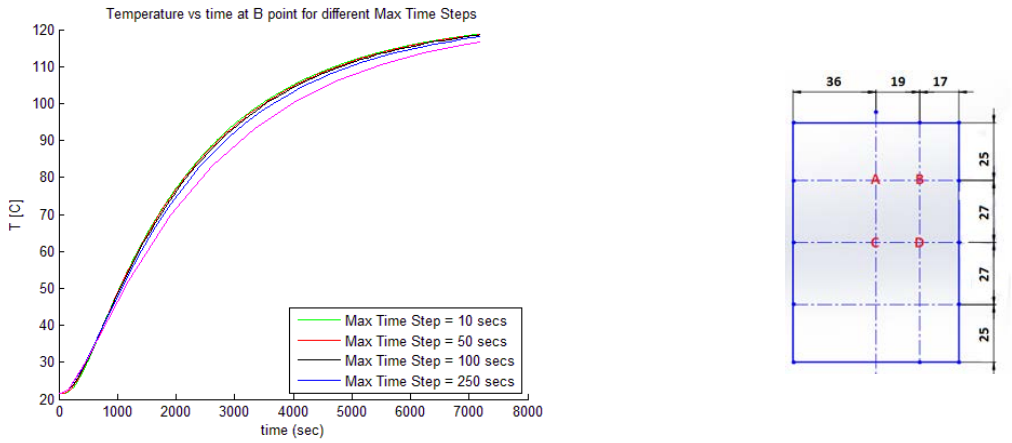

Fig. 34- Temperature vs time at B point for different maximum time steps.

Hence, the verification of the FEM analysis is made. And considering the expensive of the meshes and time costs the first obtained results is used for making comparison between FEM analysis, analytical and experimental results.

4.4 A comparison of results of the analytical method, finite element method and experimental data

In figures (35, 36, 37 and 38), time variations of temperatures which are obtained by analytical and numerical (FEM) solutions are compared with the experimental data. These solutions shows the temperature variations at the relative measuring points which are shown on the right hand side of the figure (34). It is seen that the transient thermal analysis of the analytical solution and the finite element solution via computer simulation matches very closely. However the simulation forecasts a time of sterilization larger than in real world, and it is in favor of safety.

In this particular case a better match with experiments is obtained by the simple hypothesis that external tinplate can temperature is equal to environmental T∞ since forced ventilation is quite turbulent.

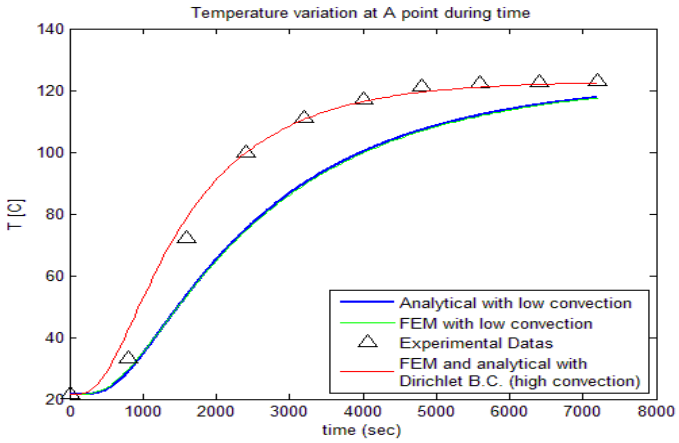

Fig. 35- Temperature variation at A point during 7200 secs.

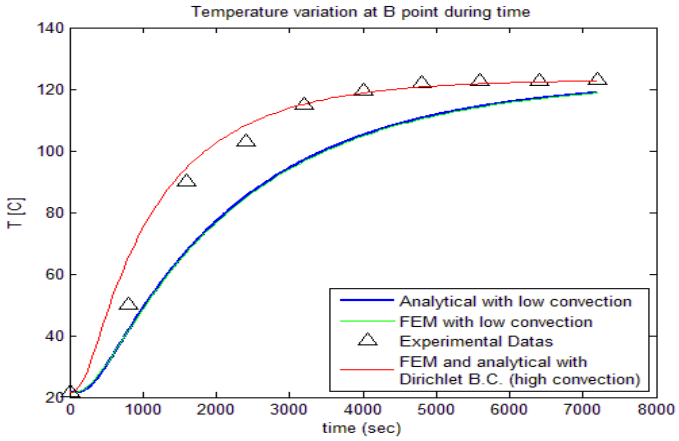

Fig. 36- Temperature variation at B point during 7200 secs.

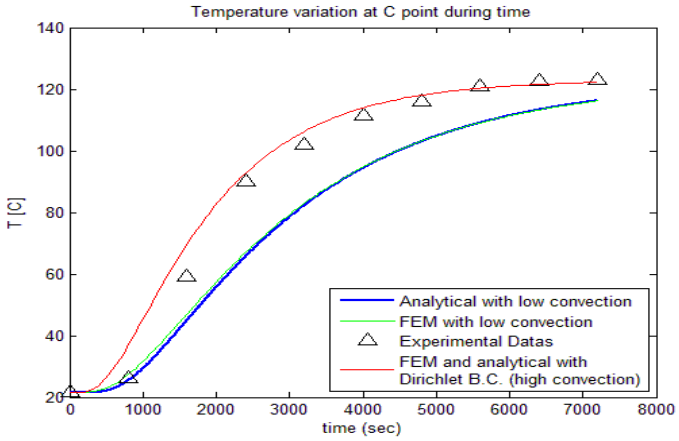

Fig. 37- Temperature variation at C point during 7200 secs.

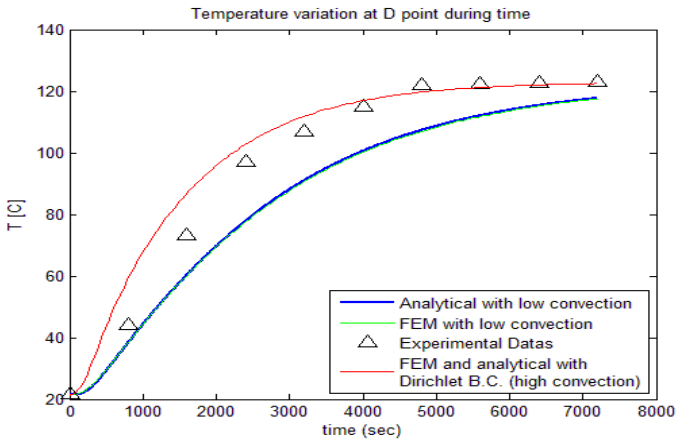

Fig. 38- Temperature variation at D point during 7200 secs.

4.5 **Conclusion**

The solid behavior of the food container is assumed and an exact analytical solution is obtained for the two-D transient temperature in a food can under sterilization at high temperature with the known initial temperature and surface heat transfer coefficient. The results are obtained in terms of a series expansion solution involving Bessel functions and based on the principle of separation of three variables. The eigenvalues required by the series expansion are obtained by root solving method by making a use of orthogonality of Bessel functions and homogeneous boundary conditions together. A not homogeneous condition brings to a Fourier analysis with an unknown coefficient left. It has been found that a finite number of roots can be used to obtain the analytical solution with reasonable accuracy. In particular 20 terms for the two-D problem were found to be sufficient.

In addition, a finite element solution is obtained with the conductivity and specific heat of the material are a mild function of temperature and isotropy is given. It is enforced the hypothesis that the heat convective forced flow is uniform all around the can and on both the caps.

Finally, a comparison is made between the analytical, numerical and experimental results. It was obtained that the finite element simulation result has a similar shape with that obtained by the conventional theoretical model. However, there is a significant difference with the experimental data, but a better match with experiments is obtained by the simple hypothesis since forced ventilation is quite turbulent.

Chapter 5

A cooled turbine blade under parallel convective and radiative heat flux, with and without internal cooling

5.1 Overview on Gas Turbines

One of the world's most salient and widespread power engineering technology is "gas turbines" (GT), either to produce power or thrust, for use in propulsion systems, power generation plants and other industrial applications.

These devices, also called combustion turbines, play a key role due to a myriad of advantages in a great variety of applications. Some of its significant advantages are having a great power-to-weight ratio, remarkable reliability, ability to run with many different gaseous or liquid fuels such as natural gas, liquefied natural gas, diesel fuel, oil and biomass gases. While having multiple fuel flexibility, however, most GTs operate on natural gas particularly in industrial applications.

The rates of their power output can vary from a few kilowatts to hundreds of mega-watts according to their ancestry, applications and the quality of the hardware. A variety of terms is used to describe the types of GT models but they are generally classified as aircraft engine type and industrial type.

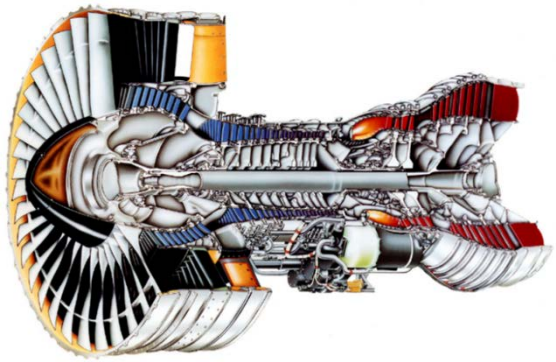

Fig. 39- Cut-away of the Pratt & Whitney PW4000-94 turbofan engine. (Source: www.pw.utc.com/PW400094_Engine)

A cut-away drawing of the PW4000-94 turbofan engine produced by Pratt & Whitney is shown in figure (39). It covers a range of 231.3 – 275.8 kN of thrust and powers several aircrafts. Figure (40) shows a commonly used industrial and marine gas turbine. The LM2500 engine is developed by GE Aviation which is a derivative of CF6 aircraft engine and its power output is approximately 25 MW.

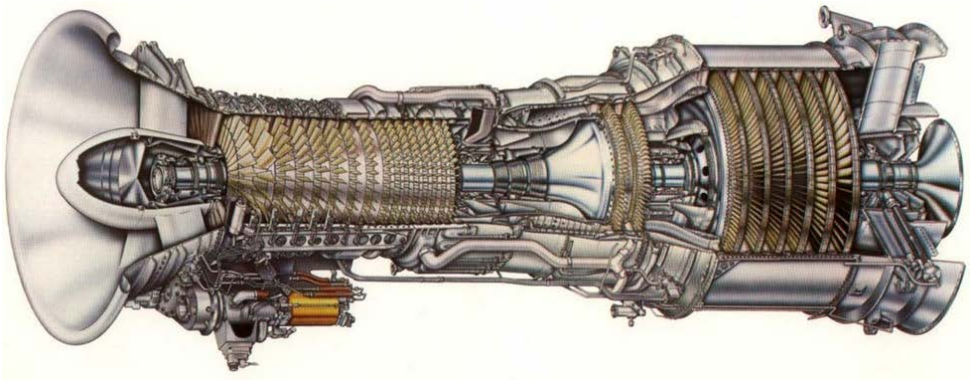

Fig. 40-- Diagram of the GE LM2500 gas turbine engine. (Source: www.ge.com)

In point of fact, both types have some things in common and share technologies driven from their designs and simulations. All gas turbines are made up of three chief components; namely a compressor, a combustor and a turbine. The arrangement of a simple open-cycle gas turbine is shown in figure (41).

The working fluid, which is usually air, is drawn into the rotating compressor and is compressed. The pressure and the temperature of the gas increase as a result of this

process. The compressed air is then heated at constant pressure in the combustor by burning fuel and air mixes, where the gas reaches to the maximum cycle temperature. Subsequently, the hot gases are expanded to the atmospheric pressure through the turbine to produce power.

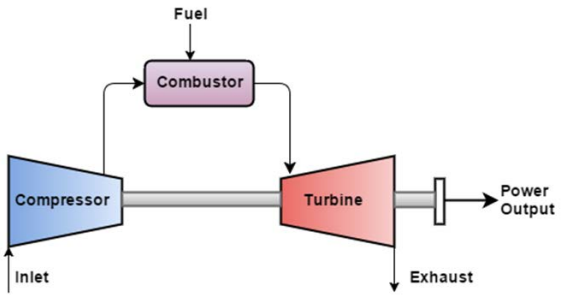

Fig. 41-- A simplified open-cycle gas turbine diagram.

However, outputs of the turbine are extracted differently for both types. In short, in the aircraft types generally the turbine acts as a windmill to drive the compressor by using the output and the hot gases are then accelerated into the atmosphere through an exhaust nozzle to produce thrust. Unlike the aircraft type, typically in the industrial types, much of the produced work by the turbine is used for the requirement of driving the compressor (back work) while the remaining is considered as the useful work via shaft power to turn an energy conversion device. In addition to this kind of simple configuration, some additional equipment can also be added in order to increase the efficiency or output of a unit such as regeneration by heat exchanger, intercooling or reheating.

Thermodynamic analyses used by gas turbines are based on Brayton, also called Joule, cycle. A P-v and a T-s diagram of the Air Standard (ideal) Brayton Cycle are shown in figure (42).

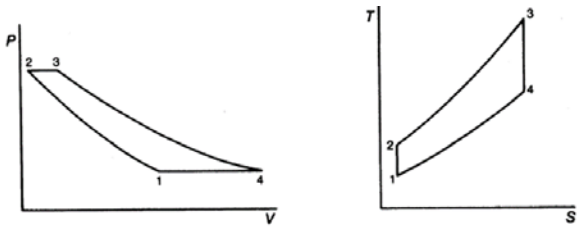

Fig. 42-– The ideal Brayton cycle.

This ideal Brayton Cycle consists of four internally reversible processes where the combustion and exhaust processes are replaced by the heat addition and the heat rejection processes at constant pressure, respectively, while compression and expansion of the gases are assumed to be isentropic. On the other hand, actual gas cycles are quite complex and differs from the ideal Brayton cycle, in which all the processes are assumed internally reversible since there are irreversibilities in the compressor and the turbine such as friction in the bearings, and pressure drop in the flow passages and combustion chamber. However, the conclusion to be drawn from the ideal Brayton cycle is that its efficiency varies with the temperature ratio which is related to its pressure ratio.

Therefore the two factors which most affect the gas turbines efficiencies are; namely, pressure ratios and temperature. For an optimum thermal efficiency, the increase of both these two factors are essential since they are in parallel to each other. Developments of the pressure ratios and the firing temperature values are shown in figures (43) and (44), respectively.

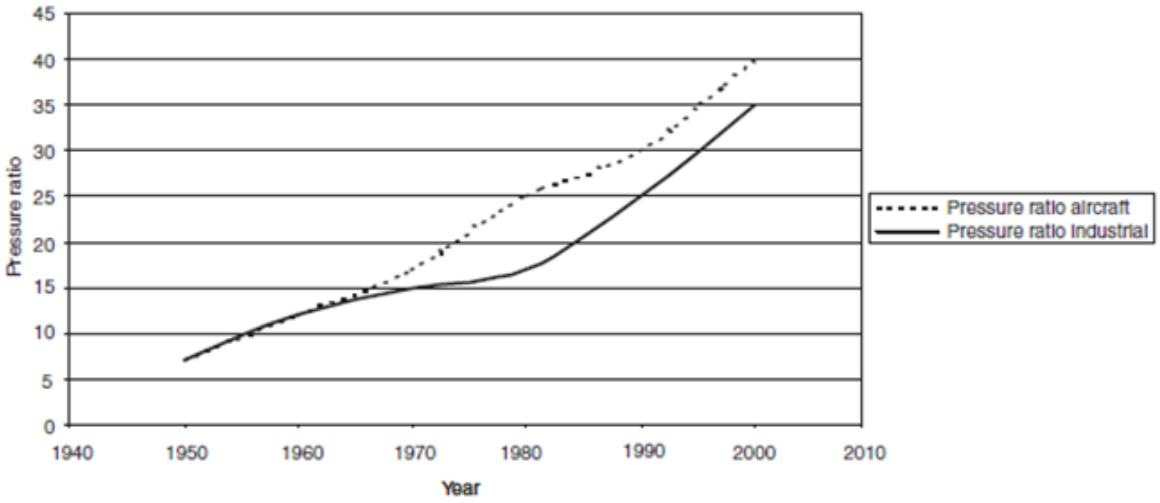

Fig. 43- The rise in pressure ratios over the years. (Source: [41])

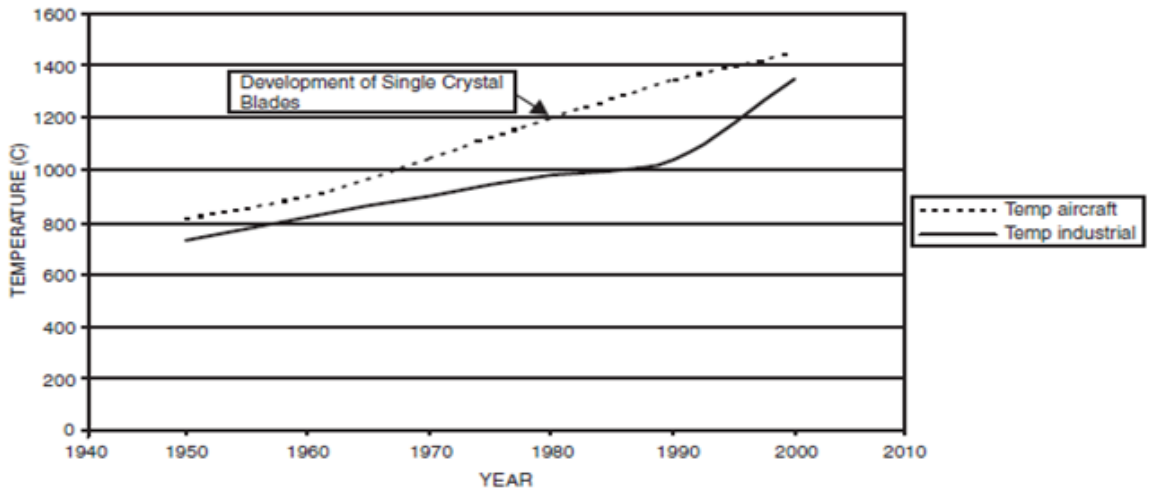

Fig. 44- The increase in firing temperatures over the years. (Source: [41])

5.1.1 **Cooling Technology and Increasing Efficiency**

The quest to increase the thermal efficiency and the power of gas turbines for the future engines, gas turbine manufacturers are trying to reach higher turbine inlet temperatures (TIT), meanwhile higher compression pressure ratios [24]. However, there is a limitation to increasing the TIT since the permissible temperature level of the cycle is limited by the softening point of the materials, and operation at very high temperatures damages the turbine and reduces the life time of the turbine vanes and blades, as the blades are under large stresses and weaker.

In advanced gas turbines of today, the hot gases enter the turbine section at a temperature of greater than 1800 [K], which is far from the melting point of the turbine blade materials. Besides, there are presently no metals or coatings which can resist to that much high values of temperatures. Therefore, turbine blades need to be cooled so they can withstand these tremendous temperatures and the maximum temperature of the cycle can be increased.

The recognition of material temperature limitations has led to the continuous turbine development programs for new materials, advanced thermal barrier coatings and cooling technologies in conjunction with their related multi-disciplinary disciplines such as fluid dynamics, heat transfer, aerodynamic, mechanical and structures, all aimed to meet the increasing demands [25]. Incorporation of the growth material

technologies and new high temperature coatings have significantly relaxed the temperature limitations. But, as their developments almost reach a culminating point, further increases in TITs can only be achieved from advanced airfoil cooling technologies [25]. As a natural consequence, the key and the most salient issue is "cooling the turbine blades" in order to ensure higher performances of the modern gas turbine engines.

Various techniques of turbine blade cooling have been proposed over the years, it is usually performed by the extracted air from the exit of the compressor. This involves a loss in the thermal efficiency, however, a considerable gain in turbine performance offsets this loss. Turbine blade air-cooling technique can be classified in two main sections; internal and external, as follows:

- *Internal cooling*: convection cooling, jet-impingement cooling, pin-fin cooling.
- *External cooling*: film cooling, transpiration cooling.

The internal convective cooling, is one of the earliest method, where the coolant is passed through several enhanced serpentine passages from hub towards the blade tip and the heat is removed from the outside of the blades. Jet impingement and pin-fin cooling methods are also considered to be a technique of internal cooling [24]. Another method of cooling the blade is external cooling, also referred to as film cooling, where the coolant is ejected out through a large number of small holes to provide a thin film cooling layer on the external surface of the blade [24]. However, in all these techniques the purpose is to keep the blade temperatures compatible within the allowable values. And a combination of these cooling techniques are generally utilized by the modern gas turbines.

In fact, only in the early 1970s research activities in the turbine heat transfer and cooling analysis began [24.] Since then, great progress has been achieved in the field of turbine technology. Figure (45) shows the change in turbine inlet temperature with cooling technologies over the years.

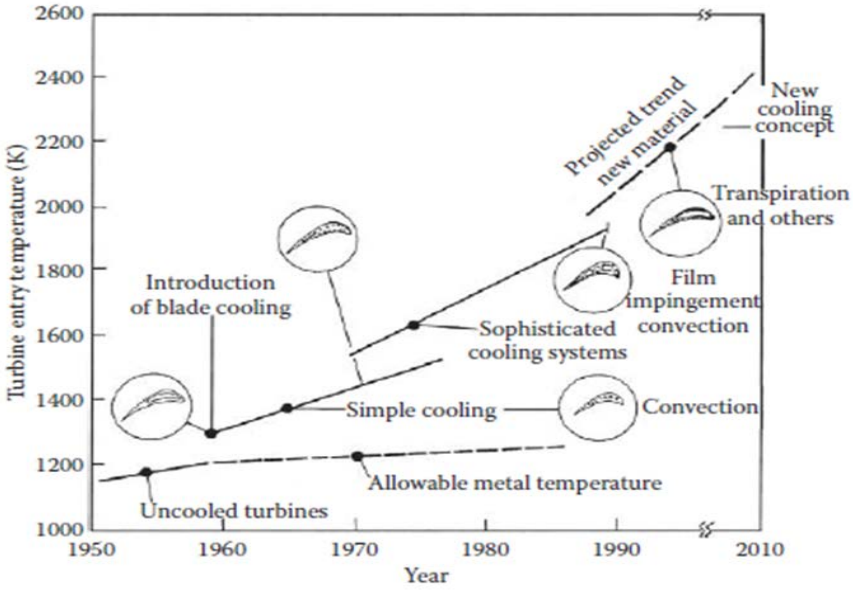

Fig. 45-- Variation of turbine inlet temperature with cooling technologies over the years. (From Clifford, 1985, collected in Lakshminarayana, B.: Fluid Dynamics and Heat Transfer of Turbomachinery. Chapter 7, pp. 597–721. 1996 [24])

5.1.2 **Motivation**

The design and the theoretical prediction of the cooling performance of internally air-cooled turbine blades is still far from being an exact science [26], since the large number of both aerodynamic and geometric variables which might influence the cooling characteristics create a considerable degree of complexity in the problem.

The proof is that in the last thirty years the gas turbine cooling technology has been based on the more detailed understanding of temperature / heat flux boundary conditions in order to solve the fluid flow field coupled with the solid energy balance equation. The way it has been done is throughout the simulation of fluid flow to get an accurate prediction of temperature field around the surface of the blade. From the computed information, boundary conditions are then shared with the solid side whose temperature distribution is solved with a solid temperature solver, such as ANSYS™. This approach is known as Conjugate Flow and Heat Transfer.

The key point of the Conjugate Flow and Heat Transfer [27], [28], [29], [30], [31],[31], 33] analysis is to simulate the turbulence and predict the laminar-turbulent transition region under transonic conditions. Consequently, a determination of the flow and

rates of the heat transfer in the laminar-turbulent transition regime is crucial, but it is quite complex since the nature of the flow is very complicated, which makes their simulation a very challenging task in the transition zone. However, in modern turbine designs, high precision transition models must be reached and experimental test data have to be collected in order to validate the analysis.

There are several methods of conjugate flow and heat transfer analysis and lots of papers have been discussed extensively [29], [30], [31], [32]. Although Large Eddy Simulation (LES) and Direct Numerical Simulations (DNS) can give accurate results in the transition zone, they are not preferable nowadays for engineering applications because of their high prices [33]. The affordable and more popular method is currently the two-equation turbulence model with transition model [33].

The result of the Computational Fluid Dynamics (CFD) simulation provides convective heat transfer coefficient in the form of Nusselt Number spatial correlation. Radiation is included in the Nusselt number as a low percent addition to the surface convection heat transfer coefficient. However, in the real GTs, radiation flux and convective heat transfer loads are in parallel and only convection is affected by laminar-turbulent transition. Nevertheless, radiation becomes the more important as the higher is the TIT.

The quantity of thermal radiation depends upon many factors such as emissivities of the blade surface exposed, absorptivity, the temperatures, including blade's sizes and shapes. It is between 10-20 % of the total heat flux already, is even higher in the regions viewing the flame zone as in the leading edge and is supposed to increase with the higher TIT.

Since the cooling system has to be designed to withstand the load peak conditions, it is of interest to assume as boundary condition the maximum radiation load that impacts on blade / vanes and the mean convective heat transfer at peak load too. By this way, an alternative method to the CHT could be to consider the thermal loads (convection and radiation) as known and investigate the conduction heat transfer in the solid side only.

5.1.3 **Objective and physical description of the model**

Accepted above assumption, a gas turbine blade is then modelled (see figure 46) which is being cooled from its base while subjected to convective and radiant heat loads from the combustion products to the its surface. The two fluxes are decoupled in the analysis as it is shown in the next section. The tip of the blade is considered to be insulated. In this way the focus was on the material thermal gradients generated by the thermal loads and on the way to distribute the cooling in order to have more isothermal behavior.

Here it is used the method to establish directly the differential form of heat contributions in terms of an appropriately chosen differential control volume, by considering that the turbine blade is made of a homogeneous metal matrix whose thermal conductivity is independent of temperature, as it was done in the previous sections for other engineering processes with explicit solutions.

As a first simpler approach, in the section (5.3), an analytical solution is obtained for the pseudo two-dimensionally temperature distribution in the turbine blade with no internal cooling process. Subsequently, a finite element analysis is made for the turbine blade under the same conditions by utilizing ANSYS™ program. And then, the comparison is made between the results those provided by the analytical solutions and by the finite element solutions. The results of these analysis is considered to be the starting point of a more elaborate procedure that takes into account the internal cooling process.

In the next section (5.4), with regard to the internal cooling, it is then introduced in the control volume the rate of energy subtraction as a distributed sink per unit volume. In this step, the strength of the energy subtraction is a key point of the investigation. It could not be uniform due to the characteristic blade shape, and has to be designed in order to bring the cooling where it is needed more. For the convenient, the terms “heat sink” or “law of cooling” are used as a description of the strength of the energy subtraction per unit volume; such strength has to be also distributed in the spatial directions. Indeed the way the blades are internally cooled by ducts and ribs properly positioned it has to follow an effective qualitative / quantitative heat subtraction strategy.

All things considered, it is expected that the model herein proposed and developed will give information to the designer on how to engineer the cooling inside the blade and, therefore, take the advantages on knowing where heat sink is more necessary.

Technically, this is modeled by the aforementioned approach throughout the mathematical formulation of the energy balance equilibrium in the workpiece, in terms of its temperature. Such balance is modeled by a quasi-two dimensional problem, whose formulation is derived in the section (5.2).

The problem is presented by the means of a degenerate elliptic partial differential equation in a rectangle, with Dirichlet, Neumann and Robin boundary conditions. Once some remarks about the problem are given, solution is concerned with its numerical resolution procedure that is obtained through the Finite Element Method (FEM) technique. Therefore, some examples and simulations are obtained and analyzed

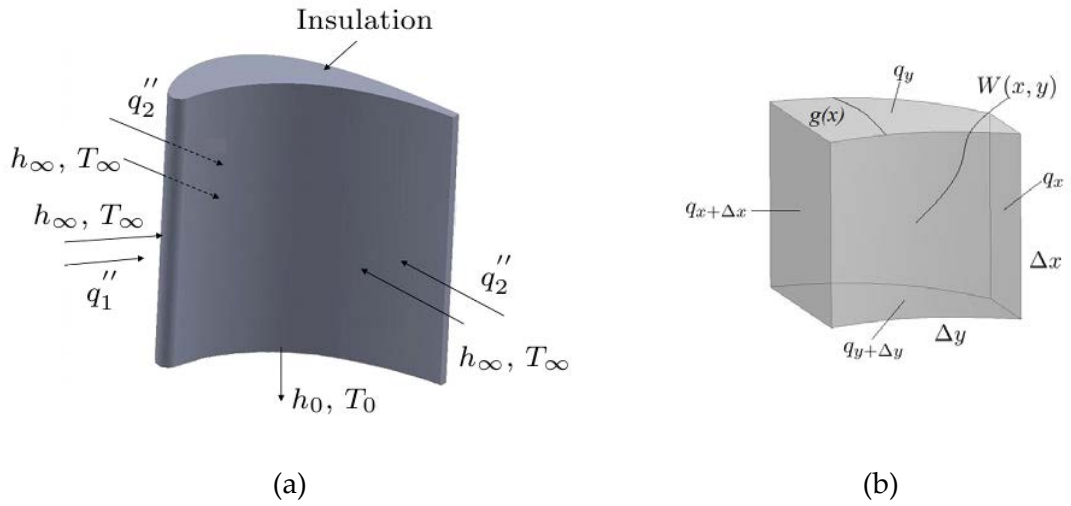

(a) (b)

Fig. 46- (a) Heat load distribution around an inlet guide vane and a rotor blade.

(b) Differential element of the blade.

5.2 Quasi 2D Energy Balance Modelling

The heat transmission by radiation requires prediction of the space-dependent concentration and radiative properties of transient species (OH CO …) and of the main products of combustion, CO_2 and H_2O, whose infrared (IR) emissivity values are function of partial pressures, of pressure ratio, of mean beam length, of gas & surface metal temperature [34], [35]. The combustion products' emissivity is related to Hottel emissivity with band overlapping correction effect [36]. The Hottel emissivities of any steady and transient species, CO_2 and H_2O mainly, with temperature as a parameter, form a family of curves of the form $\varepsilon = \mathrm{a}\, x^{\mathrm{b}} - \mathrm{c}$

Where x is the partial pressure P (atm) of species multiplied by mean free path L and a, b and c are functions themselves of temperature. An example of literature correlations [37] is as follows:

$$x = PL$$

$$\mathrm{a} = \mathrm{a}_1 \exp - \left(\mathrm{a}_2\, T\right) - \left(\mathrm{a}_3\, T\right)^{\mathrm{a}_4} \left[\sinh\left(\left(T - \mathrm{a}_5\right)/\mathrm{a}_6\right) + \mathrm{a}_7\right]$$

$$\mathrm{b} = \mathrm{b}_1 \exp\left(\mathrm{b}_2\, T\right) - \mathrm{b}_3 / \left\{\left(T\, \mathrm{b}_4\right) \cosh\left[\mathrm{b}_5 \left(\mathrm{b}_6 - T\right)\right]\right\}$$

$$\mathrm{c} = \mathrm{c}_1 / \left[\left(T / \mathrm{c}_2\right)^{(T/\mathrm{c}_3)^2 \sinh\left[\left(T - \mathrm{c}_4\right)/\mathrm{c}_5\right]}\right]$$

The combined or Hottel emissivity of the main IR absorption/emission components is then found from the relation:

$$\varepsilon_{\mathrm{g}} = C_{\mathrm{CO}_2} \varepsilon_{\mathrm{CO}_2} + C_{\mathrm{H_2O}} \varepsilon_{\mathrm{H_2O}} - \Delta\varepsilon$$

The empirical fit for Hottel charts is in [37] including Cj and correction for wave length overlapping. Convective heat transfer comes from Nusselt correlation from experimental data [38], [39]. A family of correlation as following is given:

$$\mathrm{St} = \mathrm{K}\, \mathrm{Re}^{a}\, \mathrm{Pr}^{-b}$$

From here h_∞ is inferred. The thermal load Q (Watt) could be then calculated inside a reasonable range of nowadays engineering apparatus according to the below empirical relations.

$$Q = Q_C + Q_R$$
$$Q_C = h_\infty A_C \left(T_s - T_\infty\right)$$
$$Q_R = \varepsilon_s \sigma A_R (\varepsilon_{gas} T_\infty^{\ 4} - \alpha T_s^{\ 4})$$

The following figure (47) shows the expected heat load distribution around an inlet guide vane and a rotor blade [24]. At the leading edge the heat flux is higher both for the flame proximity (direct radiation heat flux effect) and the stagnation enthalpy. As the flow splits and travel along the surface the heat flux decreases up to the point of transition from laminar to turbulent, and the heat transfer increases. The transition is expected in the suction side mainly.

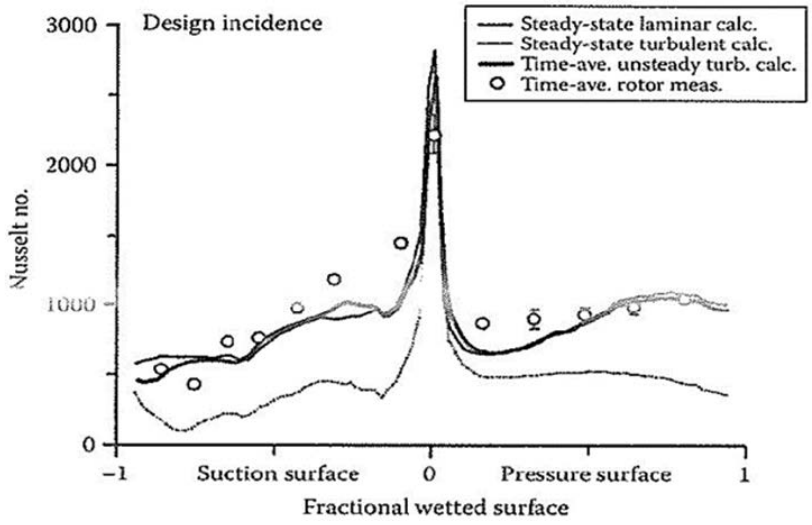

Fig. 47-- Comparison of measured heat transfer coefficients. Source: [24], [40].

To use the convective heat flux local values – as a continuous function along the curved variable - is not conceivable in order to solve analytically the energy balance in the alloy.

To write explicitly the heat balance of the first principle equation, and to solve exactly the temperature field, it appears anyway feasible to preserve partly the variability of heat flux along the curved coordinate. It is done by assigning a constant mean value of convective heat transfer along all the blade surface through T_∞, h_∞ and adding to it the radiation flux, (variable) given by Hottel charts at the boundaries. Radiation, as the convective heat flux, is then inserted into the boundary

conditions and in the first principle statement. The tip of the blade -shroud area- is assumed with almost zero heat flux in the y direction.

The case study is three dimensional, geometrically complex as shown in figure (46) and it requires a simplification to be treated analytically. Since the mean blade thickness is less than 0.01 [m] and the Biot number is below 1/6, the energy balance in the blade is modeled as a quasi-2D problem, including into the differential equation of the heat transfer load in the third direction z, convection and radiation independently [34]. The blade then has become to be considered as lumped in the transverse direction z to justify the scale down from 3-D to quasi-2-D formulation. This means that the variation of temperature in the direction of z can reasonably be approximated as being uniform.

The two heat fluxes are then defined as the following equations, where q_1'' is towards the leading side and q_2'' is towards the suction and pressure surfaces.

$$Q_{R_1} / A_{rad,leading} = q_1''$$
$$Q_{R_2} / A_{rad,sides} = q_2''$$

Statement 1 According to the basic studies on emissivity of heteropolar gases, it is possible to infer the amount of power that impinges by radiation on a gray surface (see [36]), even if it is a cumbersome procedure. A number of investigations tentative way to express analytically the Hottel charts or explores alternative ways (see [37]).

In this sense due to the high non linearity of gas radiation parameters, it is not possible to provide an explicit relationship for Q_{R1} and Q_{R2} , and therefore Q_R. We expect then that radiation Q_R on the first stage blades is around 200 W and 400 W. The leading edge is exposed to higher flux due to the proximity of the can while a lower flux hits the suction and pressure sides.

To these radiation fluxes the convective heat transfer coefficient effect h_∞, due to the high speed and turbulence inside the cascade, has to be added [35]. Even though the dependence of h_∞ is not easily expressed as an analytical function, we assume for it a reasonable value taken between 150 W/m^{2}K and 400 W/m^{2}K [33]. Therefore, the convection contribution Q_C is from 200 W to 1100 W. These ranges will be considered in the numerical examples.

5.2.1 **Internal Energy Balance Modeling**

The analytical expression of the steady energy balance, within the small volume element figure (46.b) of length Δx and height Δy, is expressed as the following equation

$$\frac{\partial}{\partial x}\left[kg\frac{\partial T}{\partial x}\right]\Delta x\Delta y+\frac{\partial}{\partial y}\left[kg\frac{\partial T}{\partial x}\right]\Delta x\Delta y+2q_2^{''}\Delta x\Delta y-2h_\infty\left(T-T_\infty\right)\Delta x\Delta y \\ -W(x,y)g(x)\Delta x\Delta y=0 \qquad [5.1]$$

where g denotes the cross section of the blade and it is idealized as

$$g\left(x\right)=\mathrm{b}\left(x/L\right)^2 \qquad (\mathrm{b}>0) \qquad [5.2]$$

Therefore equation (5.1) with constant material properties becomes

$$\frac{kb}{L^2}\frac{\partial}{\partial x}\left[x^2\frac{\partial T}{\partial x}\right]+\frac{kb}{L^2}x^2\frac{\partial^2 T}{\partial y^2}+2q_2^{''}-2h_\infty\left(T-T_\infty\right)-W(x,y)\,\mathrm{b}\left(x/L\right)^2=0 \qquad [5.3]$$

In order to make simplification following relations have been introduced

$$m^2=\frac{2h_\infty L^2}{k\mathrm{b}},\quad n=\frac{2q_2^{''}L^2}{k\mathrm{b}},\quad \tilde{W}(x,y)=\frac{x^2W(x,y)}{k} \qquad [5.4]$$

Hence, the partial differential equation expressing energy balance for the blade with internal cooling process to be solved is given in the following equation.

$$\frac{\partial}{\partial x}\left(x^2\frac{\partial T}{\partial x}\right)+x^2\frac{\partial^2 T}{\partial y^2}-m^2\left(T-T_\infty\right)=-n+\tilde{W} \qquad [5.5]$$

5.3 Analytical Solution of the cooled turbine blade under parallel convective and radiation heat flux

As a first simpler approach partial differential equation with no internal cooling process is considered and solved. The results of the analysis is considered to be the starting point of a more elaborate procedure that takes into account the internal cooling. Equation (5.5) without internal cooling process is expressed as

$$\frac{\partial}{\partial x}\left(x^2\frac{\partial T}{\partial x}\right)+x^2\frac{\partial^2 T}{\partial y^2}-m^2\left(T-T_\infty\right)=-n \qquad [5.6]$$

And the boundary conditions which are to be satisfied are given as

- b.c.1 T(0,y) = definite value since thickness is 0 at x=0.
- b.c.2 $\left.\frac{\mathrm{d}\varphi}{\mathrm{d}x}\right|_L+\left.\frac{\partial\psi}{\partial x}\right|_{L,y}=\frac{q_1^{''}}{k}-\frac{h_\infty}{k}\left[\varphi(L)+\psi(L,y)-T_\infty\right]$
- b.c.3. $\left.\frac{\partial\psi}{\partial y}\right|_{x,0}=0$
- b.c.4 $\left.\frac{\partial\psi}{\partial y}\right|_{x,l}=\frac{h_o}{k}\left[\varphi(x)+\psi(x,\mathrm{l})-T_o\right]$

Since the partial differential equation (5.6) to be solved and corresponding boundary equations are not homogeneous, separation of variables method could not be utilized. Thus, the exact solution is found through the sum of effects in the form of two functions, a pseudo 1-D solution ϕ (x), and a 2-D solution ψ (x, y) in terms of a series expansion involving Bessel function of first kind of the real order ν, as given below

$$T(\mathrm{x},\mathrm{y})=\varphi(\mathrm{x})+\psi(\mathrm{x},\mathrm{y}) \qquad [5.7]$$

And their corresponding equations are shown below, respectively.

$$\frac{\mathrm{d}}{\mathrm{d}x}\left(x^2\frac{d\varphi}{dx}\right)-m^2(\varphi(x)-T_\infty)=-n \qquad [5.8]$$

$$\frac{\partial}{\partial x}\left(x^2\frac{\partial \psi}{\partial x}\right)+x^2\frac{\partial^2\psi}{\partial y^2}-m^2\psi(x,y)=0 \qquad [5.9]$$

The equation (5.8) only in x direction is an ODE and its solution is, straight forward, given by the following equations. Firstly, it is divided into two parts; namely one is partial term and second is homogenous term as

$$\varphi(x)=\varphi_{\text{hom}}+\varphi_{part} \qquad [5.10]$$

By introducing the N constant as is equal to n + m^2 T_∞, their solution can be expressed as

$$\begin{aligned}\varphi_{part}&=N/m^2\\ \varphi_{\text{hom}}&=Ax^{r_1}+Bx^{r_2}\end{aligned} \qquad [5.11]$$

From the mathematical theory; it is known that

$$\frac{\mathrm{d}}{\mathrm{d}x}\left[x^a\frac{\mathrm{d}y}{\mathrm{d}x}\right]+y\gamma^2x^\beta=0 \quad \text{if} \quad \beta-a+2=0$$

Since this is true for the equation, the roots of function may be found with the algeabric equation as;

$$r^2+(a-1)r-m^2=0 \quad \Rightarrow \quad r_1=\frac{-1+\sqrt{1+4m^2}}{2}, \quad r_2=\frac{-1-\sqrt{1+4m^2}}{2}$$

From engineering reasoning it seems more believable the behaviour of ϕ in this way Bx^{r_1}, hence the solution of ϕ (x) results in

$$\varphi(x)=\varphi_{\text{part}}+\varphi_{\text{hom}}=N/m^2+Bx^{r_1} \qquad [5.12]$$

In order to find the constant B, the second boundary condition at x = L is applied.

$$\begin{aligned}BaL^{a-1}k+h_\infty BL^a&=q_1''-h_\infty(T_\infty-N/m^2)\\ B&=\left(q_1''-q_2''\right)/L^a\left[(ak/L)+h_\infty\right]\end{aligned} \qquad [5.13]$$

At this point, the equation (5.9) is solved by utilizing separation of variables method. A solution that is the product of two functions is assumed as following of the form.

$$\psi(x,y) = X(x)Y(y) \qquad [5.14]$$

This equation is superseded for ψ into the equation (5.9) and the following result is obtained.

$$Y(y)\frac{\partial}{\partial x}\left(x^2\frac{\partial X(x)}{\partial x}\right) + X(x)x^2\frac{\partial^2 Y(y)}{\partial y^2} - m^2X(x)Y(y) = 0 \qquad [5.15]$$
$$x^2X''Y + 2xX'Y + x^2XY'' - m^2XY = 0$$

Each term of this equation is divided by the product X(x)Y(y) and each side is set equal to a constant which result in

$$\frac{x^2X''}{X} + \frac{2xX'}{X} + \frac{x^2Y''}{Y} - m^2 = 0 \quad \Rightarrow \quad \frac{X''}{X} + \frac{2X'}{Xx} - \frac{m^2}{x^2} = -\frac{Y''}{Y} = -\lambda^2 \qquad [5.16]$$

The sign of the separation constant is chosen $-\lambda^2$ so that the eigenfunctions are obtained in direction of x. Hence the two ordinary differential equations in conjunction with their boundary conditions separately expressed as first order equations bring following solutions. Firstly, the solution for Y is given by hyperbolic functions as

$$Y''(y) - \lambda^2Y(y) = 0 \quad \Rightarrow \quad Y(y) = C_1\sinh(\lambda y) + C_2\cosh(\lambda y) \qquad [5.17]$$

Here the coefficient C_1 is killed off by applying the third boundary condition. And, the solution of X is obtained from the Bessel equations which is given by the following equations

$$x^2X'' + 2xX' + \left(\lambda^2x^2 - m^2\right)X = 0 \qquad [5.18]$$

In here, by introducing $X(x) = X^*/\sqrt{x}$ eq. (5.18) becomes

$$x^2\frac{d^2X^*}{dx^2} + x\frac{dX^*}{dx} + \left[\lambda^2x^2 - \left(m^2 + 1/4\right)\right]X^* = 0 \qquad [5.19]$$

And its solution is given by

$$X^{*}(\mathrm{x}) = \frac{1}{\sqrt{x}} C_3 J_b\left(\lambda x\right) \qquad [5.20]$$

where;

$$b = \sqrt{m^2 + 1/4} \qquad [5.21]$$

Thereby, the general form of the solution for ψ becomes

$$\psi(x,y) = \left[C_1 \sinh\left(\lambda y\right) + C_2 \cosh\left(\lambda y\right)\right]\left[C_3 x^{-1/2} J_b\left(\lambda x\right)\right] \qquad [5.22]$$

In order to determine the characteristic values of the problem, the convection boundary condition (2) is applied to the equation (5.22) and following equation is obtained by the use of the formulas for the derivatives of Bessel functions.

$$\left(-\frac{1}{2} x^{-\frac{1}{2}-1} J_b(\lambda_n x)\right)\Big|_L + x^{-\frac{1}{2}}\left(\lambda J_{b-1}(\lambda \mathrm{x}) - \frac{b}{x} J_b(\lambda \mathrm{x})\right)\Big|_L = -\frac{h_\infty}{k} \frac{1}{L^{(1/2)}} J_b(\lambda \mathrm{L})$$

And finally, the following relationship is obtained after rearranging the above equation.

$$\frac{J_b(\lambda L)}{J_{b-1}(\lambda L)} = \frac{\lambda L}{1/2 + b - Bi_L} \qquad [5.23]$$

The roots of equation (5.23) give the eigenvalues and there are infinite number of real eigenvalues as λ_1L, λ_2L, λ_3L, …..,λ_nL, which satisfy the equation (5.23). The numerical values of these eigenvalues are implemented and computed with the Matlab program. Thus the product solution of the problem is rewritten as a series expansion of kind as following

$$\psi(\mathrm{x},\mathrm{y}) = \sum_{n=1}^{\infty} C_n \cosh(\lambda_n \mathrm{y}) x^{-(1/2)} J_b(\lambda_n \mathrm{x}) \qquad [5.24]$$

Lastly, the remaining which is non-homogenous boundary condition is applied by setting y = l in equation (5.24) in order to find the C_n expansion coefficients.

$$\sum_{n=1}^{\infty} C_n \lambda_n \sinh(\lambda_n \mathrm{l}) \frac{1}{\sqrt{x}} J_b(\lambda_n \mathrm{x}) = -\frac{h_0}{k}\left[\left(\sum_{n=1}^{\infty} C_n \cosh(\lambda_n \mathrm{l}) \frac{1}{\sqrt{x}} J_b(\lambda_n \mathrm{x})\right) + \overbrace{\left(\frac{N}{m^2} + Bx^a\right)}^{\varphi(x)} - T_0\right]$$

Rearranging above equation results in

$$\sum_{n=1}^{\infty} C_n \left(\lambda_n \sinh(\lambda_n \mathrm{l}) + \frac{h_\infty}{k}\cosh(\lambda_n \mathrm{l})\right) x^{-(1/2)} J_b(\lambda_n \mathrm{x}) = -\frac{h_0}{k}\left(Bx^a + \frac{q_2^{''}}{h_\infty} + (\mathrm{T}_\infty - \mathrm{T}_0)\right) \qquad [5.25]$$

Then, a use of the orthogonality properties of the Bessel functions is made. Namely, each side of equation (5.25) is multiplied by $x^{1+1/2} J_b(\lambda_n x)$ and integrated over the x domain from 0 to L.

$$\begin{aligned} &C_n \left(\lambda_n \sinh(\lambda_n \mathrm{l}) + \frac{h_\infty}{k}\cosh(\lambda_n \mathrm{l})\right) \int_0^L x^{1+\frac{1}{2}} x^{-\frac{1}{2}} J_b(\lambda_n \mathrm{x}) J_b(\lambda_n \mathrm{x}) \mathrm{d}x \\ &= -\frac{h_0}{k}\left[\left(B\int_0^L x^{a+1+\frac{1}{2}} J_b(\lambda_n \mathrm{x})\mathrm{d}x\right) + \left(\frac{q_2^{''}}{h_\infty}\int_0^L x^{\frac{3}{2}} J_b(\lambda_n \mathrm{x})\mathrm{d}x\right) - \left((\mathrm{T}_\infty + \mathrm{T}_0)\int_0^L x^{\frac{3}{2}} J_b(\lambda_n \mathrm{x})\mathrm{d}x\right)\right] \end{aligned} \qquad [5.26]$$

Thus, the unknown values of Cn expansion coefficient is expressed as

$$C_n = \frac{\frac{h_0}{k}\left(-T_\infty + T_0 - \frac{q_2^{''}}{h_\infty}\right)\int_0^L x^{\frac{3}{2}} J_b(\lambda_n \mathrm{x})\mathrm{d}x - \frac{h_0}{k} B\int_0^L x^{a+\frac{3}{2}} J_b(\lambda_n \mathrm{x})\mathrm{d}x}{\left(\lambda_n \sinh(\lambda_n \mathrm{l}) + \frac{h_0}{k}\cosh(\lambda_n \mathrm{l})\right)\int_0^L x J_b^{\,2}(\lambda_n \mathrm{x})\mathrm{d}x} \qquad [5.27]$$

In principle, the solution of the proposed problem is completed. All the coefficients have been evaluated and they are introduced into equation (5.7) in order to obtain the temperature distribution of the turbine blade model, which results in as

$$T(\mathrm{x},\mathrm{y}) = \sum_{n=1}^{\infty} C_n \cosh(\lambda_n y) x^{-(1/2)} J_b(\lambda_n x) + \left(N/m^2 + Bx^a\right) \qquad [5.28]$$

5.3.1 **Results and Discussions of the analytical solution without internal cooling**

The following values, listed in Table (5.1), as boundaries, conductivity, convection heat transfer coefficients, gas temperature, cooling fluid temperature, radiation flux, length, height and max-thickness of the blade, are used to obtain the results.

Table 5.1- Values of the parameters used in the simulations.	
- Thermal conductivity of blade alloy	$k = 12\ (Wm^{-1}K^{-1})$
- Chord length	$L = 0.062$ (m)
- Pitch length	$l = 0.064$ (m)
- Thickness of blade	$b = 0.014$ (m)
- Convective transfer coefficient of hot gases	$h_\infty = 200\ (Wm^{-2}K^{-1})$
- Temperature of hot gases	$T_\infty = 1700$ (K)
- Convective transfer coefficient of cooling fluid	$h_0 = 1000\ (Wm^{-2}K^{-1})$
- Temperature of cooling fluid	$T_0 = 400$ (K)
- Convection flux	$q_1'' = 5\ 10^4\ (Wm^{-2})$
- Radiation flux	$q_2'' = 2\ 10^4\ (Wm^{-2})$

The above final expressions for $T(x, y)$, have been implemented in Matlab™ ambient in order to compute the results. Since the temperature is the summation of a pseudo 1-D solution ϕ (x) and an infinite series solution ψ (x, y), only a finite number of values are taken for obtaining the analytical solution of temperature distribution. The effect of λ_n roots is determined and shown in the figure (48) at two different y (height) positions = l/2 and l, respectively.

The sensibility analysis shows that 20 terms are sufficient in almost all the domain. For y = l just on the cooling lower limit in the border, the solution is affected by the number of λ_n roots. In the other points of the domain the solution converges with 20 terms already. For instance, when 40 or 50 terms are used the difference between the results is less than 0.001%.

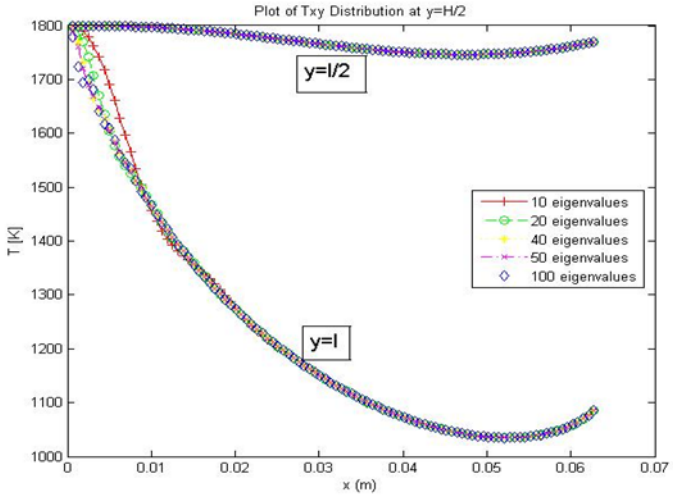

Fig. 48- T variation along x direction from different number of eigenvalues.

It is found that the pseudo 2-D solution is not accurate near the trailing edge at x = 0 where the blade idealization have no area (surface = 0 m^2), a condition not realistic from an engineering point of view.

The radiation effect forces the metal temperature to be higher than the gas temperature value T_∞. Plots of temperature distribution from these analytical results are shown in two different views in figure (49).

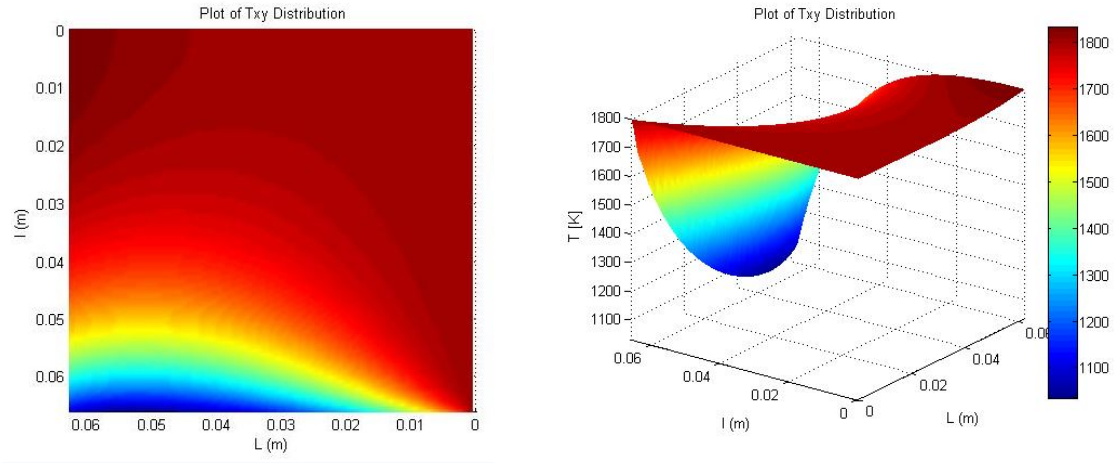

Fig. 49- Plots of Temperature distribution from the analytical solution.

From an engineering point of view we may observe that temperature is everywhere too high to preserve the material from immediate damage. Due to the low conductivity of the alloy, even with high heat transfer at the blade base, the penetration of the cooling wave is not expected to keep the metal temperature below fusion. Undoubtedly we understand the importance to insert internal cooling all over the metal and add a film cooling to internal cooling also, via discrete holes devoted to eject out compressed air. Nonetheless film cooling of the blade is out of the objective of this work.

The next development of the exact analysis will be to insert a heat sink all over the blade extension from x to L and y to l. The heat sink would be an idealization of the real internal cooling due to channel meshes.

First, a finite element analysis is made for the entire blade with no internal cooling process in order to make a comparison against the results of the analytical solution

5.3.2 **Finite Element Method Solutions without internal cooling**

The finite element analysis at the base of the code was exploited fully three dimension. The convection / radiation heat flux applied to the suction / pressure sides and leading edge were the same. Boundary condition on the trailing edge is more engineering feasible since the surface at $x = 0$ has a finite value.

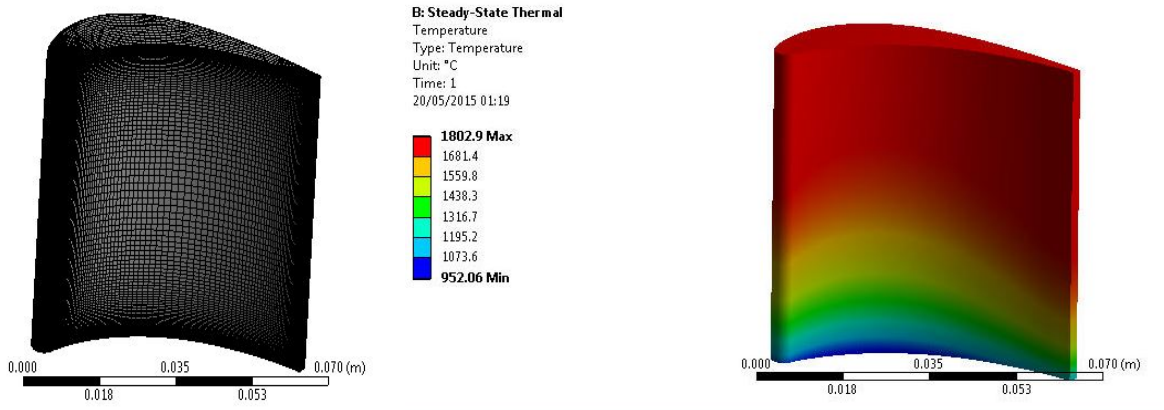

Fig. 50- The mesh structure of the blade and Temperature distribution obtained by ANSYS™.

5.3.3 **Comparison between the analytical and the numerical solutions**

The results obtained by the analytical solution were compared with those obtained numerically by a well-known powerful commercial program, ANSYS™, as illustrated in figure (51).

As it is shown, the discrepancies in temperature between numerical and analytical solution near the mid-plane y = l / 2 are still high (around 30 °C), and are more for y > l / 2. Going in the reverse direction, toward the shroud, the error is lower.

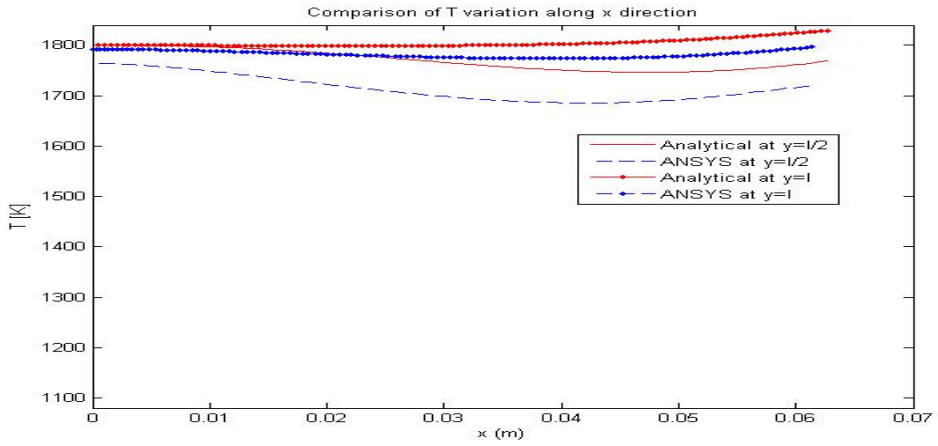

Fig. 51- Comparison of Temperature behaviour between analytical and numerical results.

5.4 **Finite element method with internal cooling**

In this section, a more elaborate procedure, which takes into account the internal convective cooling due to the use of compressor air bled from the intermediate stages of the compressor, is modelled as a sort of heat sink that allows to exceed the normal material temperature limits.

For such an hypothesis, the related energy balance already is previously derived in section (5.3), which can also be rewritten in the following form.

$$\begin{aligned}\left(kg(x)(T(x,y)-T_\infty)_x\right)_x \Delta x\Delta y+\left(kg(x)(T(x,y)-T_\infty)_y\right)_y \Delta x\Delta y \\ +2q_2^{''}\Delta x\Delta y-2h_\infty(T(x)-T_\infty)\Delta x\Delta y \\ -W(x)g(x)\Delta x\Delta y=0\end{aligned} \qquad [5.29]$$

In the equation (5.29) W denotes the rate of energy subtraction as a distributed sink per unit volume in the control volume. Such cooling is sized according to the total thermal impact Q defined in the previous sections and quantifiable from estimations of Q_R and Q_C in the statement (1). Exactly, the following relationship is considered

$$W(\mathrm{x})=\mu(\mathrm{x})\frac{Q}{V} \qquad [5.30]$$

Where μ will be later appropriately fixed and V is the volume of the blade.

More exactly, we already emphasized that Q_R and Q_C are parameters linked to the GT first stage in several aircraft engines and in power-generating units, which are present in the market.

In particular, the blade thickness goes according to a quadratic law in the curvilinear x direction. The dependence of cooling should be then strongly influenced by thickness variation. On the contrary, there is no cross section variation along y direction. Therefore, we assume a larger dependence of the cooling law by x and a weak influence by y. That is the reason we solve the energy balance with a heat sink function only of x. Of course this formulation is totally suitable to solve the problem also for two-spatial variables functions.

More precisely, following three expressions are considered :

- Sin law; $\mu_1(x) = \sin\left(\frac{4}{5}\pi\frac{x}{L}\right)$ [5.31]
- Power law; $\mu_2(x) = \left(x/L\right)^2$ [5.32]
- Root law; $\mu_3(x) = \sqrt{x/L}$ [5.33]

For each case, temperature distribution on the entire domain is analyzed and then the temperature profiles and gradients are given in the following sections.

The solutions are obtained by the software package called FreeFem++. This is a free programming language, implemented in terms of the variational of PDEs and based on finite element method.

5.4.1 **Temperature Distribution on the blade**

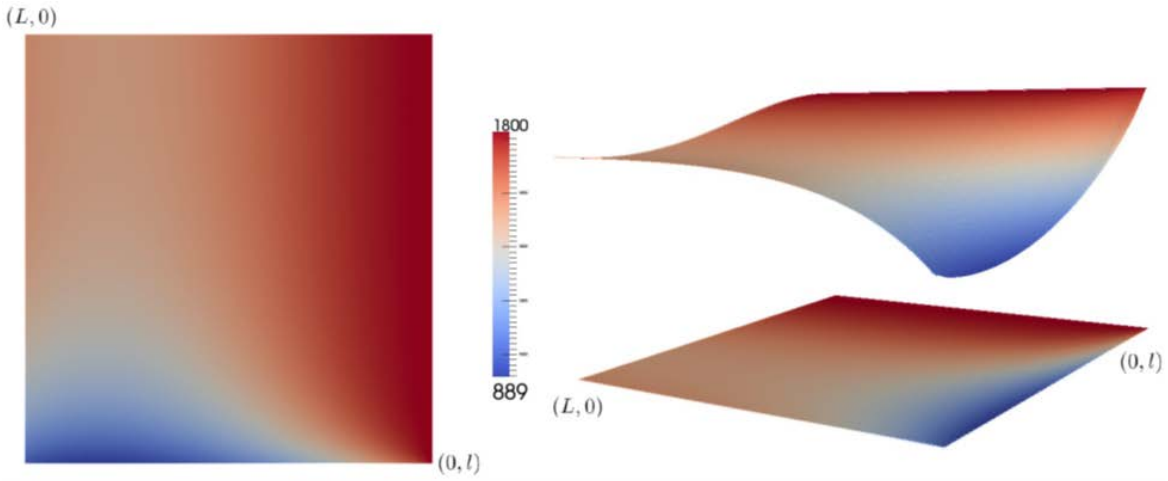

(a) Temperature distribution according to sin law.

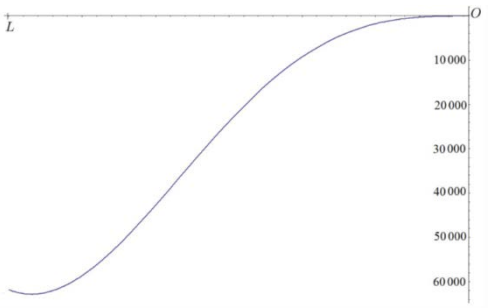

(b) Profile of the law of cooling $W_1(x)$ prescribed in equation (5.30).

Fig. 52- Temperature distribution on the entire blade for case 1; $\mu_1(x) = \sin\left(\frac{4}{5}\pi\frac{x}{L}\right)$

In figures (52, 53 and 54), the color restitutions of the temperature profiles are given in the shape of 2D graphs and 3D surface plots obtained for the three different laws of cooling explored in the analysis. The high temperature wave moves from the trailing edge inwards vertically and axially in all cases as it is not affected by any cooling. This phenomenon is expected due the singularity of the border, a sort of razor blade in the modeling, a no-surface / no-cooling flux possibly assigned.

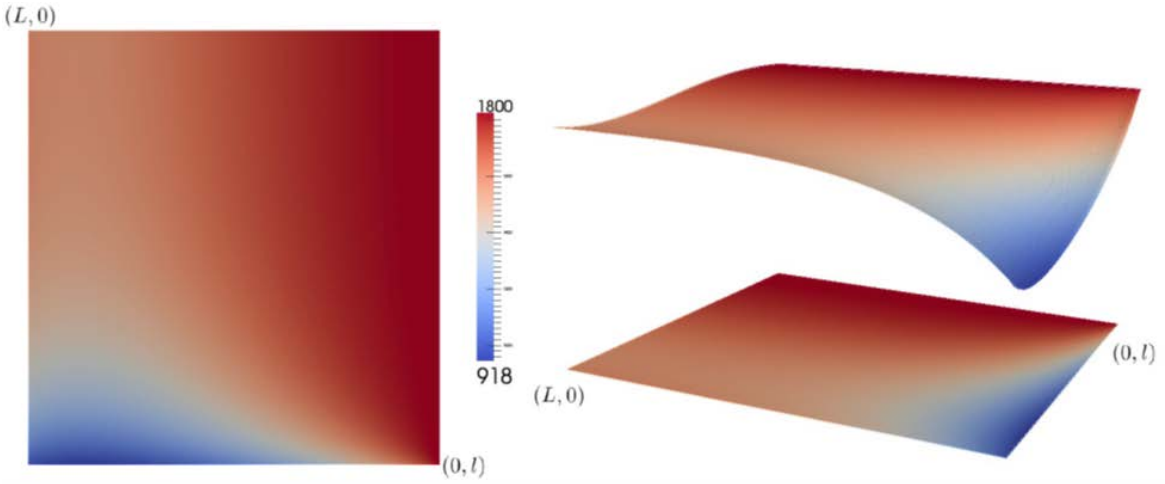

(a) Temperature distribution according to power law.

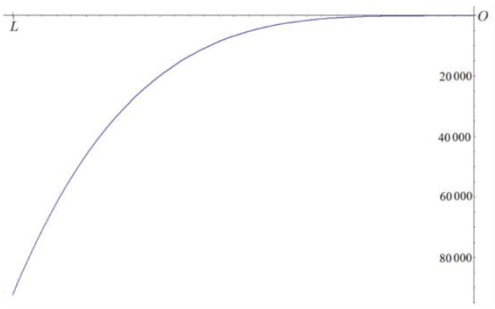

(b) Profile of the law of cooling $W_2(x)$ prescribed in equation (5.30).

Fig. 53- Temperature distribution on the entire blade for case 2; $\mu_2(x) = \left(x / L\right)^2$

Mathematically therefore the temperature at trailing edge is even higher than T_∞. In real turbomachinery the trailing edge has to be film cooled. The different formulations of heat sink shapes have no effect on this border, as they are equal zero at x = 0. An implemented analytical expression close to the border could then be studied.

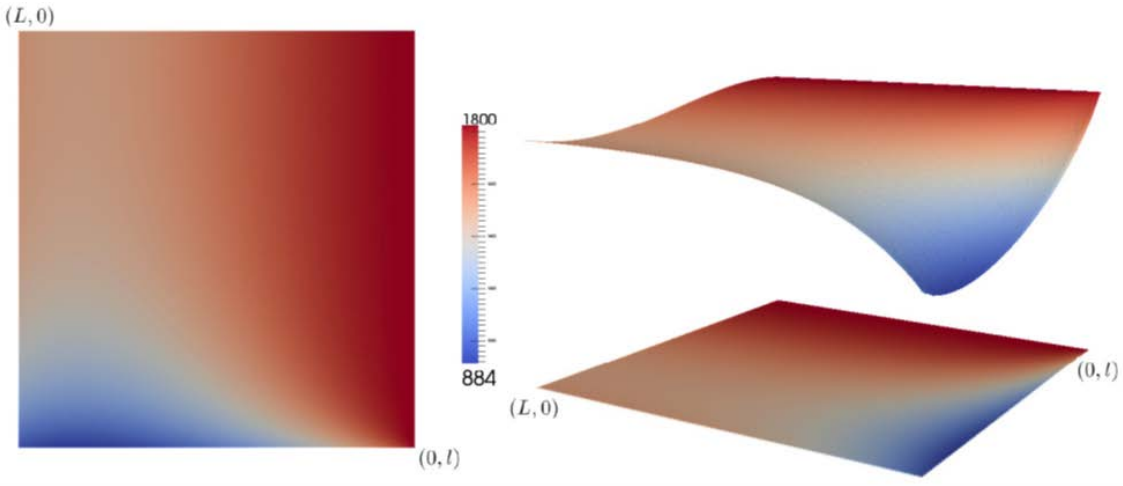

(a) Temperature distribution according to root law.

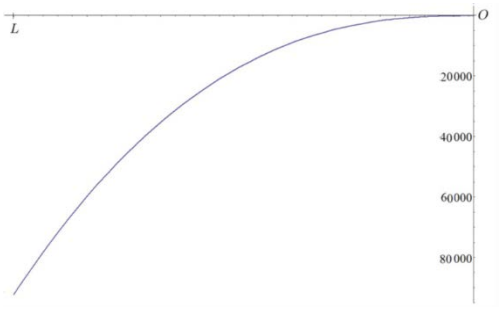

(b) Profile of the law of cooling $W_3(x)$ prescribed in equation (5.30).

Fig. 54- Temperature distribution on the entire blade for case 3; $\mu_3(x) = \sqrt{x / L}$

Staying close to the leading edge and moving inwards, apparently the progressive effect of the sin law is more effective in keeping down the hot wave than it is the power law. The root law plays itself in between, closer to sin law anyway. The penetration of the heat wave from the stagnation point on the contrary is efficiently blocked by the subtraction of heat energy given both by the cool wave from below and from the heat sink increasing with x according to functions $\mu_1(x)$; $\mu_2(x)$ and $\mu_3(x)$.

5.4.2 **Temperature profiles and gradients**

In figure (55) the values of temperature T(y) are shown in four sections taken in x = L/3; x = L/2; x = 2L/3 and x = L. The higher values of temperature are shown close to the trailing edge where film cooling is supposed to be mandatory.

Analogously, where the insulation is assumed at y = 0 position, the temperature is higher also, and decreases progressively as the cooling effect from below moves up, as a sort of cool wave that penetrates in the core blade. The values of the temperature could easily kept lower with a higher amount of heat sink. In engineering devices it would mean to implement the total cooling flow rate, and to distribute it according to the law of cooling.

The main difference in the results (in the case of T(y) versus one/thirds height plane, midplane height, two-thirds height plane and leading edge) is still found near the trailing edge border and insulation surface. In all cases temperature changes appreciably near the cooled root. For all the T(y) obtained, the ***sin law*** performs better, followed by the ***root law*** and then the ***power law*** gives apparently the poorest result in the blade core, even if tends to catch up going towards the leading edge.

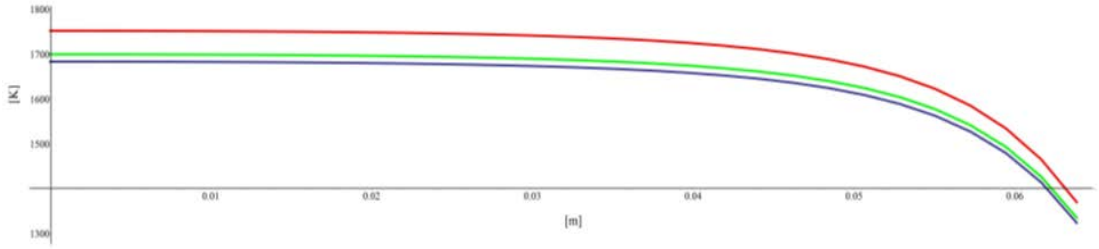

(a) Section x = L/3.

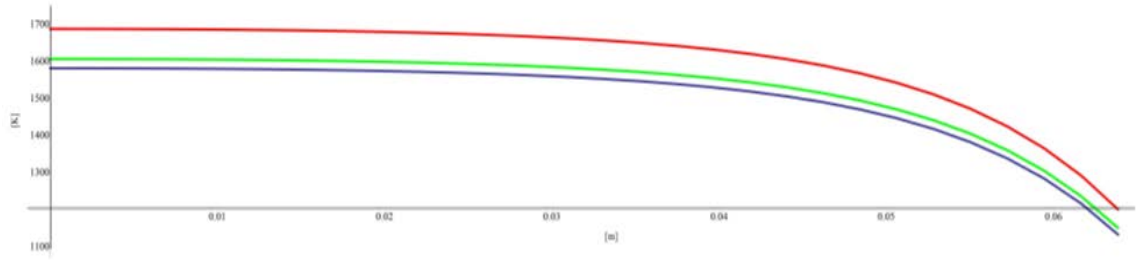

(b) Section x = L/2.

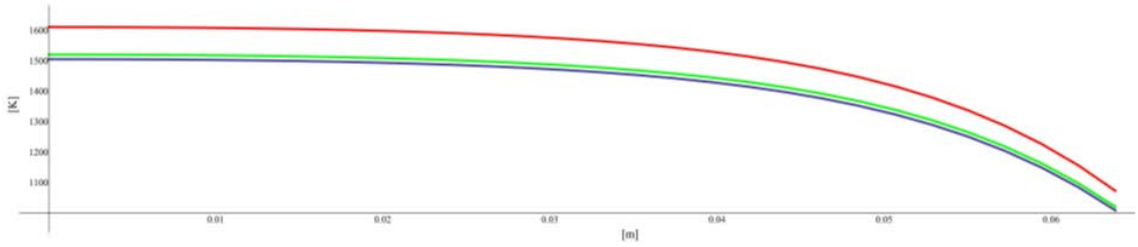

(c) Section x = 2L/3.

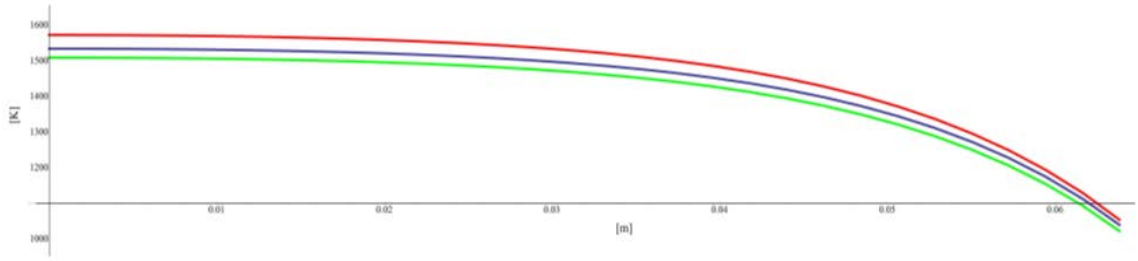

(d) Section x = L.

Fig. 55- Temperature profiles for fixed sections along x direction. The blue line represents the results in the case of the sin law ($\mu_1(x)$), the red of the power law ($\mu_2(x)$) and the green of the root law ($\mu_3(x)$).

Figure (56) shows the absolute gradients (derivatives) of T with respect to y, at flat planes taken at four different x values: L/3; L/2; (2/3) L and L. Apparently the thermal wave induced by the cooled border at y = l does not reach the alloy matrix deep into the core, as gradients are very high close to the platform.

The cool wave is able to keep metal cooled only close to the root and then, moving up towards the height center and beyond towards the adiabatic shroud, gradients become lower and temperature decisively higher. Gradients are not affected by the different law of cooling.

There are two possible explanations to this effect: the low alloy thermal conductivity and the unbalance between the amount of heat sink in the core and the thermal load induced by the cooled platform. If the gradients have to be kept lower, as it is the need, both in the model and in the real GT the balance must be reviewed.

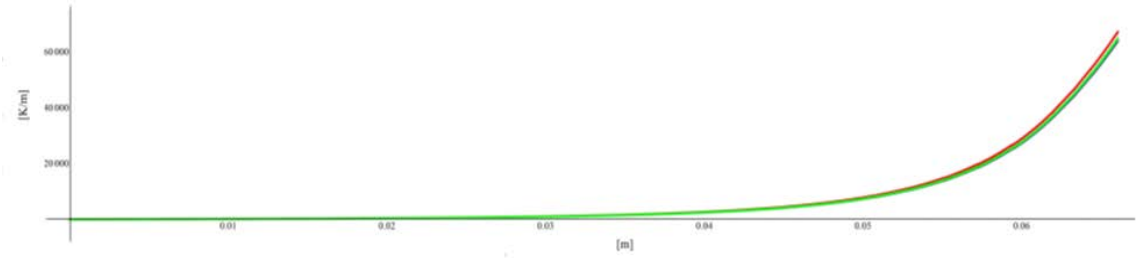

(a) Section x = L/3.

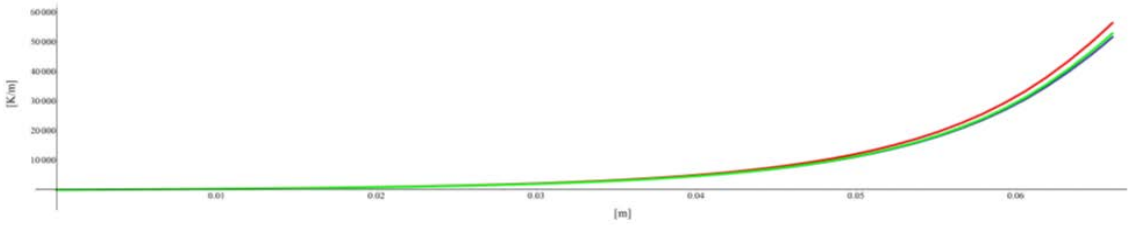

(b) Section x = L/2.

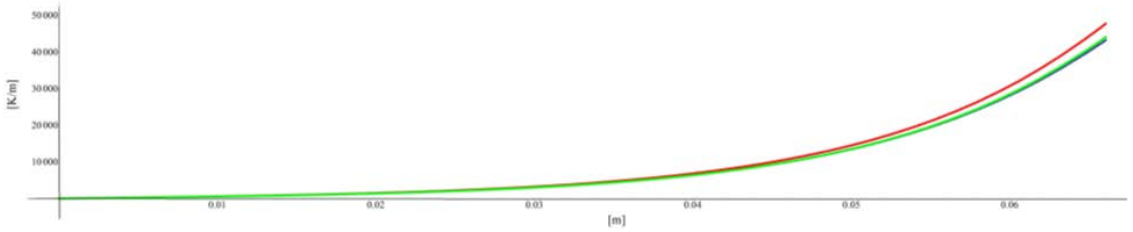

(c) Section x = 2L/3.

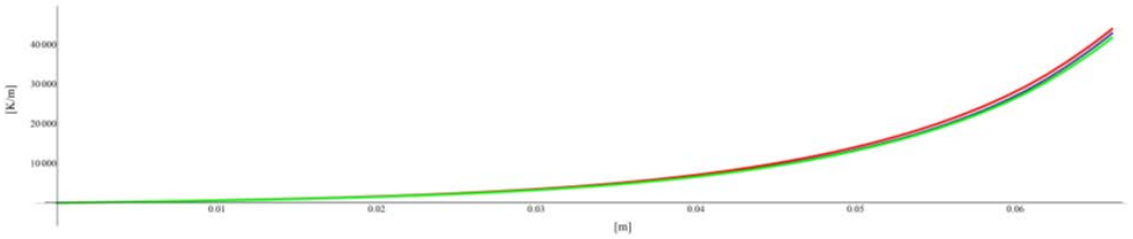

(d) Section x = L.

Fig. 56- Temperature gradients for fixed sections along x direction. The blue line represents the results in the case of the sin law ($\mu_1(x)$), the red of the power law ($\mu_2(x)$) and the green of the root law ($\mu_3(x)$).

Similarly, in figure (57) the values of temperature T(x) are shown for four sections taken in y = l/3; y = l=2; y = 2l/3 and y = l. The higher values of temperature are found close to the trailing edge, as expected. The boundary at the point x = 0, where the blade idealization have no area (in fact, the surface is 0 m^2, a not realistic condition from an engineering point of view), forces the metal temperature to be higher than the gas temperature value, i.e. equal to $T_\infty + q_2'' / h_\infty$. Even in this spatial direction the temperature absolute values could easily kept lower with an higher amount of heat sink. It would mean to implement the total cooling flow rate, and to distribute it according to the cooling law.

In the real cascade a cooling film flow has to be added at plane x = 0. The T(x) results versus one/third chord plane (at y = l/3), chord midplane (y = l/2), two-thirds chord plane (y = 2l/3) and root plane edge (y = l) are still found higher near the trailing edge surface and change appreciably as the T(x) approaches the cooled platform. Their values rise up a bit as x reaches the leading edge. For all the T(x) results the *sin law* performs better, but at the extreme stagnation point where *root law* overcomes it, followed by *root law* and then the *power law*, whose cooling effect is almost absent up to position 2/3 chord plane.

The plot reverses at about x/L = 5/8 where the *sin law* starts to decrease from the maximum value. It is the consequence of the form given to the sin law that reaches it top value at five eights of L.

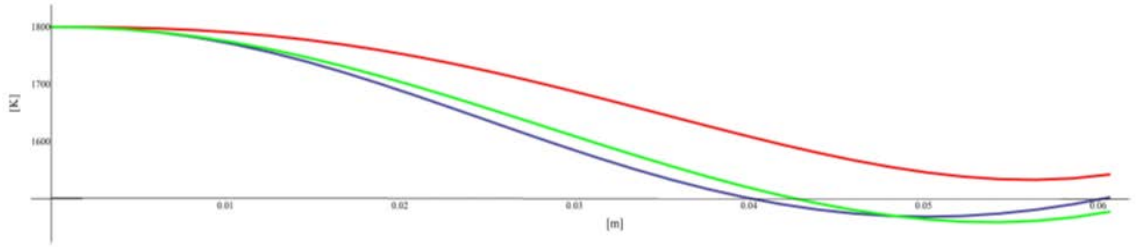

(a) Section y = l/3.

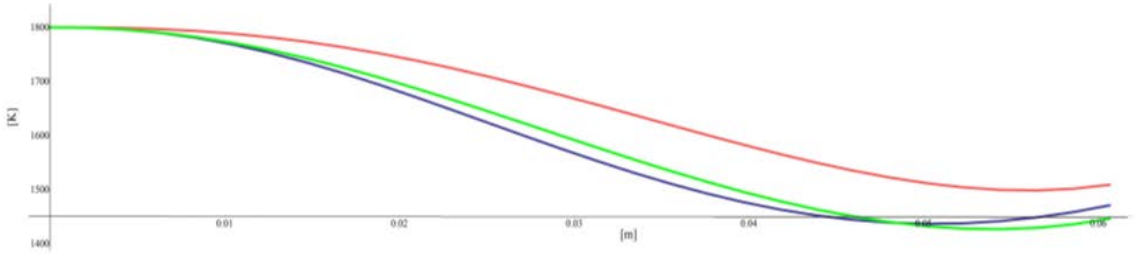

(b) Section y = l/2.

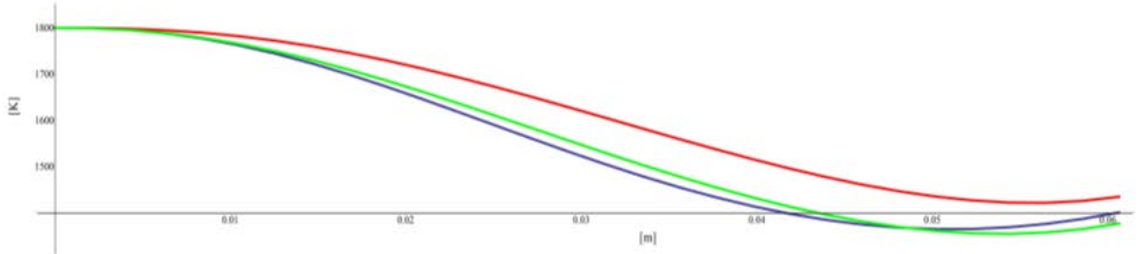

(c) Section y = 2l/3.

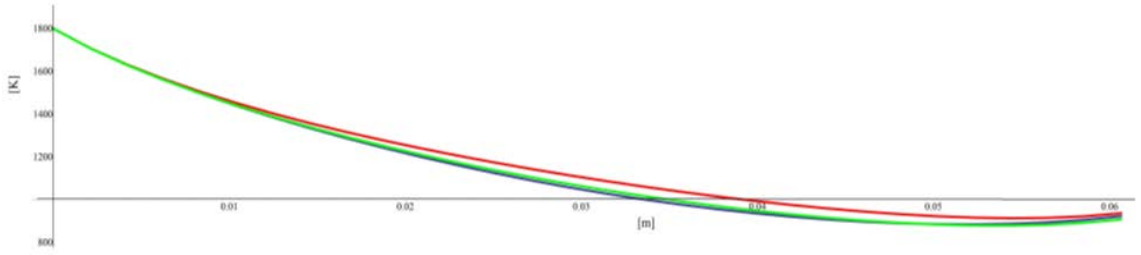

(c) Section y = l.

Fig. 57- Temperature profiles for fixed sections along y direction. The blue line represents the results in the case of the sin law ($\mu_1(x)$), the red of the power law ($\mu_2(x)$) and the green of the root law ($\mu_3(x)$).

Another observation has to be made from figure (58); here are shown the derivatives (absolute K/m) of temperature with respect to x at different constant planes: y = l/3; y = l/2; y = 2l/3 and y = l. Starting to y = l and y = 2l/3, close to the cooled lower bound, the temperature gradients are decisively low close to the trailing and leading edge and weakly dependent by the cooling low. The absolute values do not overcome the 6 (K/mm).

A different plot is given deep into the blade core: the gradients rise up and the performances of the heat sink effect are now reversed. The sin law has the lower performances at least up to x = L/2. At y = l the behavior is almost unchanged for all the three laws of cooling. As y moves away from the cooling root lower boundary, the gradient of temperature dramatically increases at midplane. Again, there are two possible explanations to this effect: the low alloy thermal conductivity and the unbalance between the amount of heat sink in the core and the thermal load induced by the cooled platform.

The best gradient performance is assigned to the *sin law* heat sink when x ≥ L/2. As the solution reaches the leading edge bound, it is possible that temperature solution is affected by the substantial increment in the heat load due to the flux q_1'' previously defined. Ultimately, noting that the apparently strong cusp at an axial distance larger than (4/5) L where gradients start to rise up abruptly from the minimum is only due to the way to return the temperature gradients as absolute values.

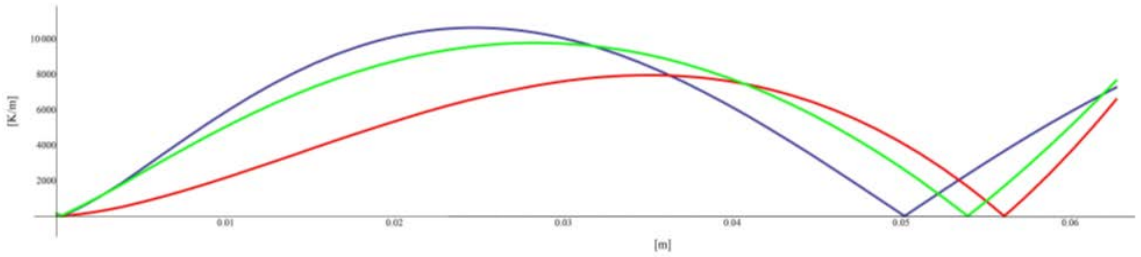

(a) Section y = l/3.

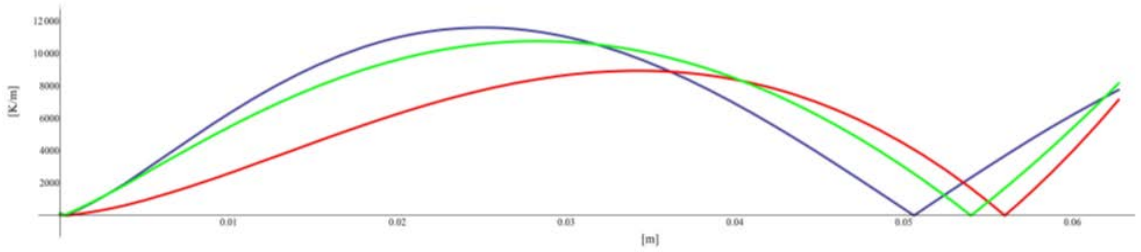

(b) Section y = l/2.

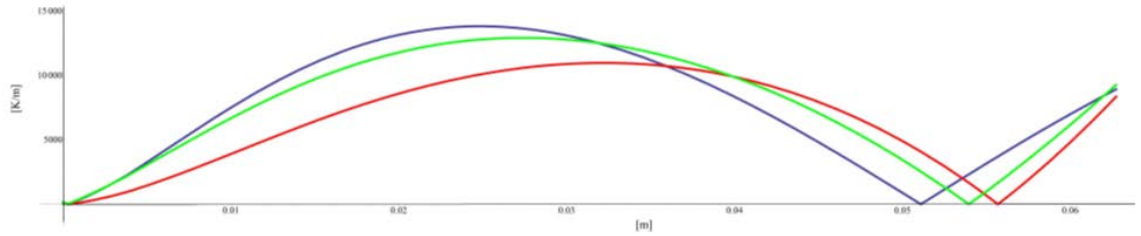

(c) Section y = 2l/3.

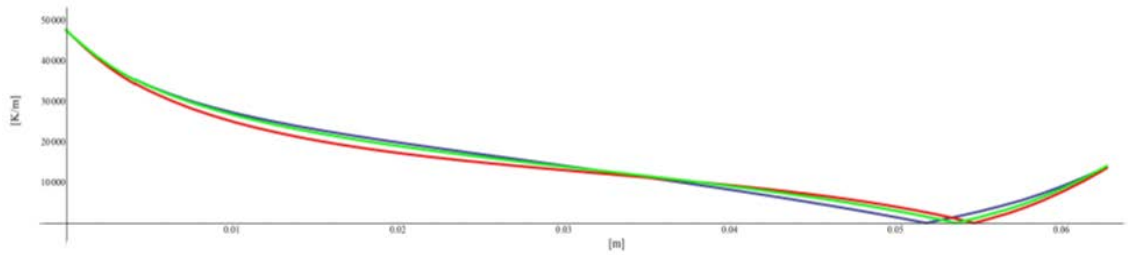

(c) Section y = l.

Fig. 58- Temperature gradients for fixed sections along y direction. The blue line represents the results in the case of the sin law ($\mu_1(x)$), the red of the power law ($\mu_2(x)$) and the green of the root law ($\mu_3(x)$).

5.5 **Conclusion**

The present work considers the first principle of energy balance, in steady, in a blade/vane gas turbine alloy affected by parallel convection and radiation heat fluxes, larger in the leading edge and lower in suction and pressure sides, cooled by convection at the platform border.

The quasi-two-dimensional approach is used as Biot number based on mean thickness is lower than 1/6 and the lumped approximation is used in the third direction z. Mathematically, the energy balance is modeled by means of a (degenerate) elliptic problem, with mixed boundary conditions (Neuman, Dirichlet and Robin), whose unknown is temperature field.

This approach tends to simplify the conjugate and heat transfer analysis of transient flow with unknown heat flow, heat transfer coefficient, laminar / turbulent, subsonic / transonic transition (to be determined), and where solutions are not available due to the uncertainty in radiative amount contribution to heat transfer and complexity of the turbulence modeling and the computation fluid dynamic analysis.

As a first simpler approach, an analytical solution is obtained for the pseudo two-dimension temperature distribution in a finite length and height turbine blade with no internal cooling process. These results are obtained in terms of series expansion which are involving Bessel functions. A method of solution is used based on the sum of the two effects: a pseudo 1-D solution ϕ (x) and a 2-D solution ψ (x, y).

It has been found that a finite number of terms can be used for obtaining the analytical solution with reasonable accuracy. In almost all the domain 20 terms were found to be sufficient. The method of solution as a combination of a pseudo 1-dimension solution ϕ (x), and a pseudo 2-dimension solution ψ (x, y) showed the domination of former with the latter part being less effective near the borders.

The comparison of the exact analysis with the full three dimension finite element modelling of the same blade by ANSYS™ shows that the analytical solution fails the more it approaches to the lower border, where it is supposed to be the cooling and it goes towards the trailing edge where the physical idealization places a surface equals to 0 m^2.

As a next step, the analytical modelling of heat transfer inside the turbine blade is considered to be implemented through a hypothesis of heat sink or "law of cooling" inside the metal, variable in accordance with the independent coordinates x and y.

These results have been the base of a more elaborate procedure that takes into account the internal convective cooling due to the use of compressor air bled from the intermediate stages of the compressor, modelled as a sort of heat sink that allows to exceed the normal material temperature limits.

Making a hypothesis on the ways metal has to be internally cooled, according to the external thermal load, a solution method of energy balance in the alloy is obtained through the finite element method. It is concluded that the FEM solution of the elliptic equation is much easier to implement as compared to the full conjugate problem to solve for both the fluid and the solid when the heat transfer coefficient and radiative flux are not known. In fact, once the partial differential problem is solved and the solution is valuable because it provides a means to infer the temperature field when a distribution of cooling effect is assigned to the domain.

Even though the numerical FEM simulations herein obtained show high values of metal temperature that in real circumstances cannot be stand, it is due only to the selected amount of thermal heat sink (negative: from -1500 W to -400 W). The lower it is the more the absolute temperature in the field decreases. However, the numerical solution presented in this research may be useful in developing a suitable numerical scheme for the conjugate problem of variable heat transfer at the boundaries and in the choice of the better law cooling devoted to keep the temperature and its gradients below excessive values.

Specifically, through this work, three hypothesis of law of cooling are investigated successfully, the differential form of heat contributions in terms of an appropriately chosen differential control volume is a valuable way to model the thermodynamic first principle, steady, at constant thermal conductivity.

The FEM solutions are easily available to the insertion of other laws of cooling function of x, or function of x and y of different fashion. The discussed results, indeed, show that the chosen laws of heat subtraction in the core and the cooling through the platform have to be better balanced. In the meantime, the heat sink in the form of power, root and sin laws are good analytical expressions to use as

starting base for improvements. As a matter of fact, in the simple form used in this work, they over-estimate the temperature in the trailing edge.

Anyway all the functions of energy subtraction in the blade the project designer would like to test, the result would be an accurate temperature distribution in the blade/vane to use as alternative or as complementary information to CHT analysis.

Bibliography

1. J.S.P.Fourier The analytical theory of heat. Cambridge University Press; 2009.
2. Arpaci VS. Conduction heat transfer. Reading, Mass.: Addison-Wesley Pub. Co.; 1966.
3. Eckert ERG, Drake RM. Analysis of heat and mass transfer. New York: McGraw-Hill; 1971.
4. Carslaw HS, Jaeger JC. Conduction of heat in solids. 2nd ed. Oxford: Clarendon Press; 1959.
5. Hahn DW, Oʹzışık MN. Heat conduction. Hoboken, N.J.: Wiley; 2012.
6. Dummer GWA. Electronic inventions and discoveries. Oxford [Oxfordshire]: Pergamon Press; 1983. p. 48.
7. Ho J, Jow TR, Boggs S. Historical introduction to capacitor technology. IEEE Electrical Insulation Magazine. 2010;26(1):20-25.
8. Jayalakshm M, Balasubramanian K. Simple Capacitors to Supercapacitors - An Overview. Int J Electrochem Sci. 2008;3:1196 - 1217.
9. Platt C. Encyclopedia of electronic components. Farnham: O'Reilly; 2012.
10. Aluminum Electrolytic Capacitors Application Guide [Internet]. Cornell Dubilier. 2007. Available from: http://www.cde.com/resources/catalogs/AEappGUIDE.pdf
11. Sclater N. Electronics technology handbook. New York: McGraw-Hill; 1999.
12. Greason WD, Critchley J. Shelf-Life Evaluation of Aluminum Electrolytic Capacitors. IEEE Transactions on Components, Hybrids, and Manufacturing Technology. 1986;9(3):293-299..
13. Huesgen T. Thermal Resistance of Snap-In Type Aluminum Electrolytic Capacitor Attached to Heat Sink. IEEE Transactions on Industry Applications. 2014;50(2):1198-1205.
14. Freiburger P. Transient thermal modeling of aluminum electrolytic capacitors under varying mounting boundary conditions. 2015 21st International

Workshop on Thermal Investigations of ICs and Systems (THERMINIC). 2015;:1-5.

15. Parler S. Thermal modeling of aluminum electrolytic capacitors. Industry Applications Conference, 1999 Thirty-Fourth IAS Annual Meeting. IEEE; 1999. p. 2418 - 2429.
16.] Parler Jr SG. Selecting and Applying Aluminum Electrolytic Capacitors for Inverter Applications. Cornell Dubilier. 2010.
17. Simpson R. Engineering aspects of thermal food processing. Boca Raton: CRC Press; 2009.
18. Kreith F. The CRC handbook of thermal engineering. Boca Raton, Fla.: CRC Press; 2000.
19. Ghani Al-Baali A, Farid M. Sterilization of food in retort pouches. New York, N.Y.: Springer; 2006.
20. Richardson P. Thermal technologies in food processing. Boca Raton, Fla.: CRC Press; 2001.
21. Mazzola P, De Clndio B, Migliali L, Massini R, Dipollina G, Pedrelli T et al. Application Of The Finite-Element Method To The Sterilization Of Canned Beef Homogenate. Industria Conserve. 1986;01:61(1):3-10.
22. Bowman F. Introduction to Bessel functions. New York: Dover Publications; 1958.
23. ANSYS Mechanical User's Guide, Release 15.0 [Internet]. 2013. Available from: http://148.204.81.206/Ansys/150/ANSYS%20Mechanical%20Users%20Guide.pdf
24. [1] Han JC, Dutta S, Ekkad S. Gas turbine heat transfer and cooling technology. New York: Taylor & Francis; 2000.
25. Cunha FJ. Heat Transfer Analysis. In: Smith L, Karim H, Etemad S, Pfefferle W. The Gas Turbine Handbook. National Energy Technology Laboratory, DOE, Morgantown, WV, 2006.
26. Ainley DG. Internal air-cooling for turbine blades: A general design survey. London: H.M. Stationery Office; 1957.

27. Han JC and Wright LM. Enhanced Internal Cooling of Turbine Blades and Vanes. In: Smith L, Karim H, Etemad S, Pfefferle W. The Gas Turbine Handbook. National Energy Technology Laboratory, DOE, Morgantown, WV, 2006. p. 312-52.

28. Bunker RS. Gas Turbine Heat Transfer: Ten Remaining Hot Gas Path Challenges. J Turbomach. 2007;129(2):193.

29. Alhajeri M, Alhamad Alhajer H. Heat and fluid flow analysis in gas turbine blade cooling passages with semicircular turbulators. International Journal of Physical Sciences. 2009;4(12):835-845.

30. Bredberg J. Turbulence Modelling for Internal Cooling of Gas-Turbine Blades [Ph.D.]. Chalmers University Of Technology; 2002.

31. Akhter MN, Ken-ichi F. Development of prediction method of boundary layer bypass transition using intermittency transport equation. International Journal of Gas Turbine, Propulsion and Power Systems. 2007;1(1):30-7.

32. Bhaskaran R, Lele SK. Heat Transfer Prediction in High Pressure Turbine Cascade with Free-Stream Turbulence using LES. 41st AIAA Fluid Dynamics Conference and Exhibit. 2011.

33. Jun Z, Qing X. Conjugate Flow and Heat Transfer of Turbine Cascades. Heat Transfer - Theoretical Analysis, Experimental Investigations and Industrial Systems. InTech; 2011.

34. McAdams WH. Heat transmission. 3rd ed. New York: McGraw-Hill; 1954.

35. Incropera FP, DeWitt DP, Bergman TL, Lavine AS. Fundamentals of heat transfer. 6th ed. New York: John Wiley & Sons; 2006.

36. Hottel HC, Sarofim AF. Radiative transfer. New York: McGraw-Hill; 1967.

37. Bueters KA, Cogoli JG, Habelt WW. Performance prediction of tangentially fired utility furnaces by computer model. Symposium (International) on Combustion. 1975;15(1):1245-1260.

38. Louis J.F.Systematic studies of Heat Transfer and Film Cooling Effectiveness. High Temperature Problems in Gas Turbine Engines, Paper 28, AGARD CP-229. 1977.

39. Sundberg J. Heat Transfer Correlations for Gas Turbine Cooling [Magister]. Linköping University; 2006.

40. Abhari RS, Guenette GR, Epstein AH, Giles MB. Comparison of Time-Resolved Turbine Rotor Blade Heat Transfer Measurements and Numerical Calculations. J Turbomach. 1992;114(4):818.

41. Boyce Meherwan P. Gas engineering handbook. Boston: Gulf. Prof. Publ; 2006.

42. Chen X, Liu Y. Finite element modeling and simulation with ANSYS Workbench. CRC Press; 2014.

43. Madenci E, Guven I. The finite element method and applications in engineering using ANSYS. New York: Springer; 2006.

44. Bergheau JM, Fortunier R. Finite element simulation of heat transfer. London: ISTE Ltd.; 2008.

45. Crank J. The mathematics of diffusion. 2nd ed. Oxford: Clarendon Press; 1975.

46. Lakshminarayana B. Fluid dynamics and heat transfer of turbomachinery. New York: Wiley; 1996.

47. Weigand B. Analytical methods for heat transfer and fluid flow problems. Berlin: Springer; 2004.

48. White RE. Computational Mathematics: Models, Methods, and Analysis with MATLAB and MPI. Chapman and Hall/CRC; 2003.

49. Li J, Chen Y. Computational partial differential equations using MATLAB. Boca Raton: CRC Press; 2009.

50. Lyshevski S. Engineering and scientific computations using MATLAB. Hoboken: Wiley-Interscience; 2003.

51. Goswami DY. The CRC handbook of mechanical engineering. 2nd ed. Boca Raton, Flor.: CRC Press; 2004.

52. Sun D. Computational fluid dynamics in food processing. Boca Raton: CRC Press; 2007.

53. Toledo RT. Fundamentals of food process engineering. New York, NY: Springer; 2007.

54. Ciafone JD. Gas turbines: technology, efficiency, and performance. Hauppauge, N.Y.: Nova Science Publisher's; 2011.

55. Giampaolo T. Gas turbine handbook. 4th ed. Lilburn, GA: Fairmont Press; 2011.

56. Cohen H, Rogers GFC, Saravanamuttoo HIH. Gas turbine theory. 4th ed. Burnt Mill, Harlow, Essex, England: Longman Scientific & Technical; 1996.